High Energy Physics, Vienna, 1968, edited by J. Prentki and J. Steinberger (CERN, Geneva, 1968).

[10]S. O. Holmgren, S. Nilsson, T. Olhede, and N. Yamdagni, Nuovo Cimento 57A, 20 (1968).

[11]G. Goldhaber, W. B. Fowler, S. Goldhaber, T. F. Hoang, T. E. Kalogeropoulos, W. M. Powell, Phys. Rev. Lett. 3, 181 (1959); G. Goldhaber, S. Goldhaber, W. Lee, and A. Pais, Phys. Rev. 120, 300 (1960).

[12]Aachen, Berlin, Bonn, Hamburg, München Collaboration, Nuovo Cimento 42A, 954 (1966).

[13]Bonn, Durham, Nijmegen, Paris (E.P.), Turin Collaboration, Phys. Rev. 161, 1356 (1967).

[14]J. Bartke, O. Czyżewski, J. A. Danysz, A. Eskreys, J. Loskiewicz, P. Malecki, J. Zaorska, K. Eskreys, K. Juszczak, D. Kisielewska, W. Zielinski, M. Szeptycka, K. Zalewski, G. Pichon, and M. Rumpf, Phys. Lett. 24B, 163 (1967); M. Bardadin-Otwinowska, M. Danysz, T. Hofmokl, S. Otwinowski, H. Piotrowska, R. Sosnowski, M. Szeptycka, A. Wroblewski, Institute of Nuclear Research, Warsaw Report INR NO. 761/VI/PH, 1966 (unpublished).

[15]P. Daronian, A. Daudin, B. Gandois, C. Kochowski, L. Mosea, CERN Report No. 68-7, Vol. 2, 1968 (unpublished).

[16]K. Bockmann, H. Drevermann, K. Sternberger, N. Stief, T. Hofmokl, L. Michejda, S. Otwinowski, H. Piotrowska, R. Sosnowski, M. Szeptycka, W. Wojeik, and A. Wroblewski, Institute of Nuclear Research, Warsaw Report "P" No. 837/VI/PH, 1967 (unpublished).

[17]S. O. Holmgren, S. Nilsson, T. Olhede, and N. Yamdagni, Nuovo Cimento 57, 20 (1968).

[18]W. DeBaere, J. Debaisieux, E. DeWolf, P. Dufour, F. Grard, P. Herquet, J. Heughebaert, L. Pape, P. Peters, F. Verbeure, G. Charriere, D. Drigard, W. M. Dunwoodie, A. Eskreys, Y. Goldschmidt-Clermont, A. Grant, V. P. Henri, F. Muller, Z. Sěkera, and J. K. Tuominiemi, Nucl. Phys. B22, 131 (1970).

[19]O. Czyżewski and M. Szeptycka, Phys. Lett. 25B, 482 (1967).

[20]Bruxelles-CERN-Cracow Collaboration, A. Eskreys et al., Nucl. Phys. (to be published).

[21]J. W. Elbert, A. R. Erwin, and W. D. Walker, Phys. Rev. D 3, 2043 (1971).

[22]S. L. Stone, D. Cohen, M. Farber, T. Ferbel, R. Holmes, P. Slattery, and B. Werner, Nucl. Phys. B32, 19 (1971).

[23]W. Ko and R. L. Lander, Phys. Rev. Lett. 26, 1064 (1971).

[24]O. Czyżewski, in *Proceedings of the Colloquium on Multiparticle Dynamics, University of Helsinki, 1971*, edited by E. Byckling, K. Kajantie, H. Satz, and J. Tuonminiemi (Univ. of Helsinki Press, Helsinki, 1971).

[25]C. E. DeTar, Phys. Rev. D 3, 128 (1971).

[26]K. C. Moffeit et al., Phys. Rev. D 5, 1603 (1972).

[27]L. Caneschi, Phys. Rev. D 3, 2865 (1971).

[28]J. H. Friedman and C. Risk, Phys. Rev. D 5, 2245 (1972). ,

[29]M. Duller and W. D. Walker, Phys. Rev. 93, 215 (1954); G. Cocconi, Phys. Rev. 111, 1697 (1958).

[30]T. F. Hoang, Nucl. Phys. B38, 333 (1972).

[31]M. A. Abolins et al., Phys. Rev. Lett. 25, 126 (1970).

[32] Aachen-Berlin-Bonn-CERN-Cracow-Heidelberg-Warsaw-Collaboration, in *Proceedings of the Amsterdam International Conference on Elementary Particles, 1971*, edited by A. G. Tenner and M. Veltman (North-Holland, Amsterdam, 1972).

Large-Angle Quasielastic Electron-Deuteron Scattering*

K. M. Hanson,[†] J. R. Dunning, Jr.,[‡] M. Goitein,[§] T. Kirk,[‖] L. E. Price,[**] and Richard Wilson

Harvard University, Cambridge, Massachusetts 02138

(Received 28 September 1972)

Measurements of differential cross sections for quasielastic electron-deuteron scattering $e + d \to e + p + n$ have been made in which recoil protons were detected in coincidence with the scattered electrons. The ratios of the elastic electron-neutron to the electron-proton scattering cross sections are derived from the proton coincidence data. For comparison, these ratios are also determined from the scattered-electron momentum spectra using the peak and area methods. The theory developed by Renard, Tran Thanh Van, and LeBellac, which includes corrections for the final-state interactions, is found to explain the proton coincidence results. The present measurements, made at an electron scattering angle of 90° for four-momentum transfers of $q^2 = 7$, 10, 15, and 29 F^{-2}, and at 80° for $q^2 = 45$ F^{-2}, are combined with previous results to obtain the electromagnetic form factors of the neutron.

I. INTRODUCTION

The quasielastic electron-deuteron process $e + d \to e + n + p$ has been investigated. The aim of the measurements presented here is to provide information about the electric and magnetic form factors of the neutron, G_{En} and G_{Mn}. The present experiment extends the proton coincidence method used by Budnitz et al.[1] to large electron-scattering angles.

In the proton coincidence method, protons which recoil in the direction of momentum transfer are detected in coincidence with scattered electrons. Quasielastically scattered electrons which possess protons in coincidence, "ep events," arise mainly from the interaction of the electron with the proton

in the deuteron nucleus. Those which have no proton coincidence, "e$\overline{p}$ events," arise mainly from the electron-neutron interaction. Thus it is possible to relate the experimental ratio e$\overline{p}$/ep to the ratio of the elastic e-n to the elastic e-p scattering cross sections σ_n/σ_p (σ stands for the differential cross section $d\sigma/d\Omega$). The theoretical corrections needed to obtain σ_n/σ_p from the proton coincidence data are discussed in Sec. II. The effects of the final-state interactions (FSI) between the outgoing neutron and proton on the interpretation of the data are found to be significant.

A brief review of the various types of measurements which have been made to determine the neutron form factors is given by Budnitz *et al.*[1] The proton coincidence method offers many experimental advantages over other techniques. These are: increased statistical precision for the same number of electrons detected, few and relatively small experimental corrections, and complete insensitivity to the calibration of the electron spectrometer, as well as other systematic uncertainties. Although the emphasis in the present experiment is on the proton coincidence method, the data are also analyzed by two additional techniques which do not use the proton coincidence: the area method and the peak method. The area method compares the integrated quasielastic electron momentum spectrum to the hydrogen cross section σ_p. The peak method compares the double-differential cross section $d^2\sigma/d\Omega\,dE'$ at the peak of the quasielastic spectrum to σ_p. The momentum spectrum of electrons possessing proton coincidences may also be analyzed using these methods to provide a test of the theory used to interpret the data.

In conjunction with the present experiment, elastic electron-proton scattering cross sections were measured using a liquid hydrogen target. The e-p results have already been reported by Price *et al.*[2] The hydrogen data serve to cali-

brate the apparatus for the deuterium measurements. By reporting the results of the area and peak methods in terms of ratios to the e-p measurements, many systematic uncertainties common to both the D_2 and H_2 measurements are eliminated.

The kinematic parameters associated with each datum point are given in Table I.

The deuteron theory used to interpret the data is discussed in Sec. II. Section III describes the apparatus. The analysis of the data is covered in Sec. IV and the experimental results are presented in Sec. V. The neutron form factors obtained from the combination of previous quasielastic e-d measurements with the present results are given in Sec. VI.

The notation used in the present work is the same as used by Budnitz *et al.*[1] with the exception that E'_{peak} always refers here to the elastically scattered electron momentum from protons. Further details concerning the present experiment may be found in Ref. 3.

II. DEUTERON THEORY

A. Cross Sections Without Final-State Interactions

A theoretical expression for the triple-differential cross section $d^3\sigma/d\Omega\,dE'd\Omega_p$ is needed in order to interpret the proton coincidence results of the present experiment in terms of the proton and neutron form factors. Two theories which provide expressions for the triply differential cross section have been used in the present analysis, one due to McGee[4] and the other to Renard, Tran Thanh Van, and LeBellac.[5]

McGee[4] extends the earlier work of Durand[6,7] by including small relativistic corrections in his calculation. He obtains the relativistic corrections by starting with a relativistic covariant dispersion theory. Employing the relation between

TABLE I. Kinematic parameters of data points (given for elastic electron-proton reaction).

q^2 (F^{-2})	q^2 (GeV/c)^2	Electron angle, θ (deg)	Incident electron energy, E (GeV)	Scattered electron energy, E'_{peak} (GeV)	Proton angle, θ (deg)	Proton kinetic energy, T_p (GeV)
7.0	0.273	90	0.449	0.304	34.1	0.145
10.0	0.389	90	0.557	0.350	32.1	0.208
15.0	0.584	90	0.718	0.407	29.5	0.311
20.0	0.779	90	0.865	0.450	27.5	0.415
28.76	1.120	90	1.104	0.507	24.7	0.597
45.0	1.752	80	1.598	0.664	23.8	0.934

the spectral functions and the nonrelativistic deuteron wave functions found by Blankenbecler and Cook,[8] McGee is able to write the cross section in terms of these wave functions. The relativistic corrections are calculated only to order q^2/M_p^2. However, they remain very small throughout our range of q^2.

The formulas used here to evaluate McGee's theory are the same as those stated explicitly by Budnitz.[1] The importance of using k_n, the laboratory momentum of the neutron (or proton), instead of $|\vec{p}^* - \frac{1}{2}\vec{q}^*|$ in evaluating the cross sections should be reemphasized. The modified Hulthèn model of the deuteron wave functions is used here, too, since it allows some of the necessary integrals to be done analytically (see Appendix A). However, the parameters used in this model have been altered slightly to take into account a new and somewhat different value for the triplet effective range.[9] The value of $\rho(-\epsilon, -\epsilon)$ used here 1.774 ± 0.007 F instead of Budnitz's value of 1.742 F. The parameters for the modified Hulthèn model obtained by using this new value and the values $Q = 0.282$ F^2 and $P_D = 5\%$ (the same as those used by Budnitz) are: $N^2 = 0.7867$ F^{-1}, $\alpha = 0.2317$ F^{-1}, $\beta = 1.642$ F^{-1}, sin$\epsilon = 0.0276$, and $\mu' = 3.242$. The results obtained with this model differ only slightly from those obtained with Budnitz's 5% D-state model. The use of these new parameters increases the theoretical value of $d^2\sigma/d\Omega\, dE'$ at the quasielastic peak by 0.6% and the area above $E' = 0.80\, E'_{\text{peak}}$ by 1.0% at $\theta = 90°$. The fraction of protons accepted by the proton counters is changed by less than 0.1% in the region of the quasielastic peak.

A convenient means of comparing the peak cross sections obtained by different authors is offered by an approximation found by Durand.[7] At the quasielastic peak, defined as $p^* = \frac{1}{2}q^*$ (or $E' = [(E - \epsilon)/E]\, E'_{\text{peak}}$), the S-state contribution to the cross section may be approximated above $q^2 = 7$ F^{-2} by

$$\frac{d^2\sigma}{d\Omega\, dE'} = \left(\frac{d\sigma}{d\Omega}\right)_{\text{Mott}} \frac{M_n M_p P^*}{\pi W^*}\left[(AG_{E_p}^2 + BG_{M_p}^2)\right.$$
$$\left. + (AG_{E_n}^2 + BG_{M_n}^2)\right]\frac{2C}{P^{*2}},$$

(1)

using the notation of Budnitz et al.,[1]

$$\left(\frac{d\sigma}{d\Omega}\right)_{\text{Mott}} = [\alpha^2 \cos^2(\tfrac{1}{2}\theta)]/[4E^2 \sin^4(\tfrac{1}{2}\theta)],$$

and A and B are the same coefficients as those appearing in the Rosenbluth cross section[10] for elastic e-p scattering: $A = 1(1 + \tau)$ and $B = \tau/(1 + \tau) + 2\tau \tan^2(\tfrac{1}{2}\theta)$, where $\tau = q^2/4M^2$. The constant C

is mainly dependent upon the deuteron model used in the calculation. For the model used in the present work, $C = 0.01485$ MeV^{-1} (S state only). It is found that the net contribution to the peak cross section from other terms (predominantly from the D-state terms) varies between 0.8% at $q^2 = 7$ F^{-2} and 1.3% at the high-q^2 points. These results are in agreement with those obtained by Braess and Kramer.[11] Their value of C (including only the S-state term) is 0.01472 MeV^{-1} for their best potential (No. 8), which is only 0.9% less than the value quoted above. This difference is attributable to their lower value of N^2 and larger P_D (5.6%). They calculate an additional contribution of about 1.1% from other terms (not including final state interactions). It should be noted that Durand's peak cross section [Eq. (84), Ref. 7] is about 2% lower than ours, mostly due to the somewhat smaller triplet effective range assumed by him.

B. Final-State-Interaction Corrections

The above discussion pertains to McGee's deuteron theory without the inclusion of the effects of final-state interactions (FSI). McGee has developed a formulism for including FSI effects.[12] His formulism is difficult to implement, however, and has not been attempted in the present analysis. That FSI effects might be important in the interpretation of proton coincidence data has already been indicated in the experimental work of Budnitz et al.[1] In a simple model where the effect of FSI is to rescatter the recoil proton from the spectator neutron, the fraction of proton coincidences is reduced by about $\sigma_{np}/4\pi\langle r^{-2}\rangle$, where σ_{np} is the total n-p cross section and $\langle r^{-2}\rangle$ is the mean inverse-square separation between the nucleons in the deuteron. This order of magnitude estimate places the size of FSI effects on the proton coincidence results integrated over the entire quasielastic spectrum at about 10%. The effect is expected to be smaller at the quasielastic peak, since it is here that the nucleons in the initial state are nearly stationary and hence, from the uncertainty principle, are furthest apart.

Fortunately the theory of Renard, Tran Thanh Van, and LeBellac[5] treats the effects of FSI on the triple-differential cross section and was available in the form of a computer program. Their theory is based on a completely covariant Mandelstam representation. Unfortunately their theory is not very transparent since it is presented in terms of projections onto 18 Lorentz-invariant forms. The Born term, which does not include FSI, takes into account the deuteron, proton, and neutron pole terms. The requirement of gauge invariance leads

to the partial inclusion of meson-exchange terms.
The FSI corrections are obtained by applying dis-
persion relations to the multipole amplitudes up to
a total angular momentum of $J = 3$ (53 multipole
amplitudes). The dispersion relations are evalu-
ated by the Omnès method under the restriction of
elastic unitarity and ignoring coupling between
states of different L. Since inelastic states have
been excluded from the unitarity condition, this
method is valid only up to about $q^2 = 17$ F^{-2}. Also,
the n-p phase shifts used in the program limit its
validity to q^2 below 17 F^{-2}.

A comparison between the triple-differential
cross sections predicted by McGee's theory and
that of Renard *et al.* at $q^2 = 10$ F^{-2} is shown in Fig.
1. ω^* is the angle between the outgoing proton
direction and $\vec{q}$ in the center-of-mass of the final
nucleons. The effect of FSI is to reduce the for-
ward and backward peaks, corresponding to the
major proton and neutron terms, respectively,
and to fill in the valley between them. This may
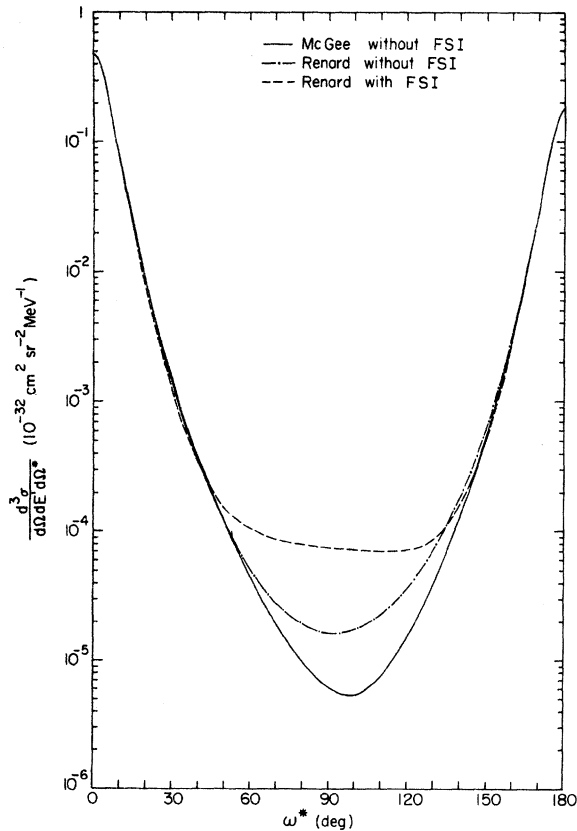be seen qualitatively as a scattering-out effect.

FIG. 1. Angular distribution of protons in the center-
of-mass system of the final-state nucleons at $q^2 = 10$ F^{-2},
$\theta = 90°$ for E' at the quasielastic peak. The meson ex-
change term is omitted from the calculation of Renard
et al.

In the present experiment the electron-proton
coincidence events, ep's, measure the integral of
the cross section over $d\Omega_p^*$ from $\omega^* = 0°$ to $43.4°$
(for the kinematic conditions represented in Fig.
1), whereas all electron events, e's, measure the
entire integral from $0°$ to $180°$. Thus FSI decrease
the fraction of electron events which have a proton
in coincidence $f_p = (ep)/e$. At $q^2 = 10$ F^{-2} the theo-
retical correction factor for the proton coinci-
dence data,

$$R = \left(\frac{\sigma_p}{\sigma_n + \sigma_p} \right) \Big/ f_p , \qquad (2)$$

is given by the McGee theory as 1.0054. The
theory of Renard *et al.* predicts $R = 1.0199$ without
FSI and $R = 1.0259$ when FSI are included. The
meson-exchange terms have been excluded in this
calculation for reasons stated below. Their inclu-
sion would reduce the value of R by about 0.7%
for the above case.

Several difficulties arise when one tries to re-
late the results of Renard *et al.* to those obtained
by other authors. Their meson exchange term
has a substantial effect on the cross section, in
contrast to what has been stated by other au-
thors.[4,7,11] This term increases the peak cross
section by about 4% at $q^2 = 10$ F^{-2} and becomes
dramatically larger as q^2 is decreased. Since
only a portion of the meson-exchange diagrams
are included, this part of the calculation of
Renard *et al.* is somewhat dubious. The meson-
exchange term has been excluded altogether from
the calculation in the present analysis. Another
unexpectedly large term is the deuteron pole term.
Its effect is to decrease the peak cross section
by about 1% at $q^2 = 10$ F^{-2}. Hughes *et al.*[13] estimated
this term to contribute less than 0.1% above q^2
$= 7.5$ F^{-2}. The deuteron-pole term has not been
dropped from the present calculations.

The normalization of the Renard *et al.* theory
is not understood. When the meson-exchange,
deuteron-pole, and FSI contributions are omitted,
their results are supposed to correspond to those
of the usual nonrelativistic theory. Yet, it is
found that the peak cross sections given by their
theory without these terms are a constant 3%
larger than our calculations of McGee's cross
sections over a large range of q^2 and θ. When the
difference in deuteron wave functions assumed in
the two calculations is taken into account, this
difference is increased by about 1.3%, leaving
a total unresolved discrepancy of more than 4%.

Because of the above stated problems in the
theory of Renard *et al.*, we are prompted to use
our calculation of the McGee theory — which is
more transparent — to interpret our single-arm
data in the peak and area method analysis. A

separate correction for FSI must therefore be made. At about $q^2 = 10$ F^{-2}, $\theta = 90°$, the FSI corrections to the peak cross section given by various authors are: Durand,[7] -1%; Nutall and Whippman,[14] -1.3%; Braess and Kramer,[11] -2.0%; Renard et al.,[5] -3.7%. For the peak method results, we will make a -2.0% FSI correction to the McGee results at all q^2 points. For the area method results, no FSI correction will be made.

Although certain doubts have been cast on the normalization of the calculations of Renard et al., their theory is found to predict fairly well the observed variation of f_p with E' (see Sec. V). Budnitz et al.[1] found at $\theta = 20°$ that this variation could not be accounted for by the McGee theory without FSI. However, a substantial amount of the variation of f_p with E' predicted by the theory of Renard et al. persists when FSI contributions are excluded from their calculations. The reason for this is not clear. It should be noted that an important advantage of the proton coincidence method is that it is insensitive to uncertainties in the overall normalization factors in the theory. The theory of Renard et al. will be used to analyze the proton coincidence data.

III. APPARATUS

The layout of the apparatus is depicted schematically in Fig. 2. An electron beam, extracted from the Cambridge Electron Accelerator, was directed at a 3.3 cm-long liquid deuterium (or hydrogen) target. Scattered electrons were detected by a scintillation counter telescope. The unscattered electron beam was monitored simultaneously by a secondary emission monitor (SEM) and a Faraday cup.

The electron spectrometer consisted of a simple quadrupole magnet which focussed electrons onto a set of momentum defining counters C1-C16. The configuration of these counters[2] divided the momentum acceptance of the spectrometer ($\Delta p/p = 25\%$) into 13 momentum bins, each about 2% wide. The FWHM (full width at half maximum) momentum resolution varied between 2.3% and 3.6%, excluding the effect of the finite bin size. The angular acceptance of the spectrometer was defined in two places. A set of tungsten jaws in front of the quadrupole determined the vertical acceptance and a pair of scintillation counters mounted on the rear edge of a lead aperture placed behind the quadrupole determined the horizontal acceptance. The solid angle of the spectrometer was about 8.3 msr at the center of the momentum bite and varied slightly with momentum. Electrons were identified by means of their characteristic responses in a gas Cherenkov counter and shower counter. The gas Cherenkov counter was filled with Freon C318 at a pressure of 20 in. Hg. absolute. The shower counter was a lead-Lucite sandwich with 9 lead sheets, each 0.5 radiation lengths thick. Following the shower counter, there were an additional 17.5 radiation lengths of lead behind which were placed a pair of scintillation counters. These counters were useful in identifying charged pions.

The proton counter telescope consisted of three large scintillation counters which subtended up to 450 msr. These counters were shielded from low-energy background by a weak magnetic field produced by a sweeping magnet. The phototube bases and coincidence electronics used for these telescope counters were chosen to provide stable operation at high instantaneous rates, typically 20
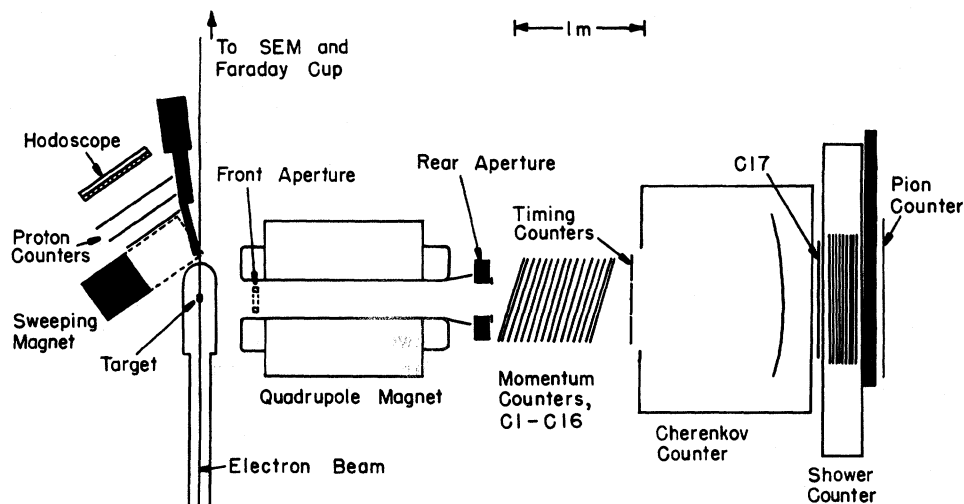
FIG. 2. Schematic layout of the apparatus.

MHz. A 12×16 element scintillation-counter hodo-
scope yielded the angular distribution of the recoil
protons.

An on-line PDP-1 computer was used to record
each event on magnetic tape. The computer was
triggered when the momentum-defining counters
indicated that a charged particle crossed the mo-
mentum focal plane of the electron spectrometer
simultaneously with the presence of a pulse in
either the Cherenkov counter or the shower coun-
ter. The information recorded by the computer
included the status of all counter discriminators
and the pulse heights measured in various impor-
tant counters, e.g., in the Cherenkov and shower
counters.

Further details regarding the apparatus may be
found in Refs. 2 and 3. The apparatus used in the
present experiment is similar in construction to
that described in more detail in Ref. 15. Thus,
many of the comments made there apply equally
well to this experiment.

IV. DATA ANALYSIS

The procedure used to analyze the data presented
here is similar to that used in Ref. 1. Those
events which represent detected electrons must be
identified and the electron's momentum deter-
mined. Various backgrounds are subtracted from
the data to isolate the quasielastic *e-d* process.
The cross sections obtained after applying appro-
priate correction factors to the accepted events
are then compared with theoretical predictions.
Throughout the analysis procedure, those events
associated with an electron-proton coincidence,
ep's, are handled separately so that after all cor-
rections are made to the data, the fraction of
electrons which have a proton in coincidence, f_p,
can be determined.

At each value of q^2, data runs were taken using,
alternately, hydrogen and deuterium targets.
Normally, H_2 runs were taken both before and
after the D_2 runs. The elastic *e-p* process ob-
served in the H_2 runs provided a valuable calibra-
tion of the response of the apparatus. Auxiliary
runs were usually taken on D_2 with the spectrom-
eter momentum bite centered 15% above and
below the quasielastic momentum peak. Runs
were also taken with the target empty in order to
allow subtraction of the contribution to the data
from the target end-walls. In addition, various
other types of background runs were taken which
will be discussed below.

A. Electron Identification

Electrons are identified as those events which
meet the following requirements: (a) large pulse
heights in both the Cherenkov and shower coun-
ters, (b) acceptable pattern in the momentum-de-
fining counter array, and (c) no pulse in the veto
counters which define the rear aperture. The
lower cutoffs on the pulse heights in the Cherenkov
and shower counters are chosen to be as low as
possible, consistent with removing unwanted back-
grounds. The detection efficiencies corresponding
to the chosen cuts are determined from the data.
For the H_2 runs, this is done by observing the
complete spectrum of the counter in question for
high energy electrons identified with the elastic
e-p process. Thus the analysis is restricted to
the prominent peak regions in the electron momen-
tum, proton time-of-flight, and proton hodoscope
distributions. A typical shower counter spectrum
obtained by this procedure is shown in Fig. 3(a).

The above procedure cannot be used for the D_2
runs. So the efficiencies for the D_2 data are ob-
tained by comparison of the Cherenkov and shower
counter spectra with those from the H_2 runs. It
is necessary to determine the efficiencies sepa-
rately for different regions of the momentum bite
of the spectrometer as well as for different set-
tings of the central momentum. The cuts chosen
for the final analysis resulted in efficiencies
ranging from 86% to 99% for the Cherenkov coun-
ter and from 76% to 93% for the shower counter.
The uncertainty in the combined efficiencies is
less than 3%.

The electron's momentum is determined on the
basis of the on-off pattern of the momentum-de-
fining counters. Most of this analysis is performed
by the PDP-1 computer using the general tech-
nique described in Ref. 15 The computer can un-
ambiguously assign the momentum bin to 97% of
the accepted events. About 86% of the accepted
events have perfect patterns (code 00 in the nomen-
clature of Ref. 15). A small fraction of the events
have patterns which are ambiguous or unrecogniz-
able to the computer. These events are either
assigned a momentum bin or rejected on the basis
of scanning them by eye. It is estimated that less
than 1% of the good electron events are rejected
in this process.

B. Background Subtraction

The contributions from electron scattering from
the 0.04 mm-thick aluminum end caps of the target
were measured in separate empty target runs.
The empty-target (ET) background is directly sub-
tracted from the prime data runs. This subtraction
amounts to about 4% of the H_2 cross section.

The elastic *e-d* scattering contributions are sub-
tracted using previously measured deuteron form
factors.[16,17] This process contributed at most 0.5%

to the area under the quasielastic e-d spectrum.

A significant background in the D_2 runs arises from the electroproduction of the $N^*(1238)$ resonance of pions. The electron momentum spectrum expected for the N^* is calculated using Adler's dispersion theory.[18] The Adler cross sections are folded with the theoretical radiated quasielastic electron-deuteron spectrum to include the effect of the internal motion of the proton and neutron inside the deuteron, as well as radiative corrections. The over-all normalization of the N^* spectrum is adjusted at each q^2 above 15 F^{-2} to obtain the best fit to the observed momentum spectra. For the purpose of correcting the coincidence data, the fraction f_p for the N^* contribution is assumed to be independent of E'. Values for this ratio between 0.2 and 0.3 seem to fit the data well. The systematic error in the N^* subtraction is taken to be $\frac{1}{5}$ its value.

An analysis of samples of the deuterium used in this experiment indicated that the only significant impurity present was $(1.5\pm0.5)\%$ HD. The D_2 data presented here are corrected for this small contamination.

The background contributions arising from the pions are determined from special background data runs. The most important type of background run is the reverse field run during which the polarity of the quadrupole magnet is reversed. The reverse field runs measure directly the contamination arising from neutral pions as well as from other charge-symmetric backgrounds. The response of the background to the insertion of a thin sheet of lead in front of the spectrometer as well as to a variety of other conditions indicates that most of the events measured in the reverse field runs come from neutral pions. The neutral pion contamination in the prime data runs is removed by a direct subtraction of the reverse field run data. This subtraction amounts to 1% to 2% for the D_2 cross sections and slightly less for H_2. Figure 3(b) shows the effect of the reverse-field subtraction on the shower counter spectrum for D_2 at $q^2 = 29$ F^{-2}. At $q^2 = 29$ F^{-2}, where the ratio of charged pions to electrons is about 30:1, the contamination from charged pions is estimated from the data to be about 0.5% of the electron rate. The size of the backgrounds from both charged and neutral pions determined from the data are in substantial agreement with calculations (Ref. 3) based on the interaction of the charged pions or γ rays (from the neutral pions) with the inside walls of the spectrometer.

Analysis of the H_2 data uncovers the existence of a background in the form of excess proton anti-coincidence events, $e\bar{p}$'s. These events remain in the tails of the momentum distribution after the
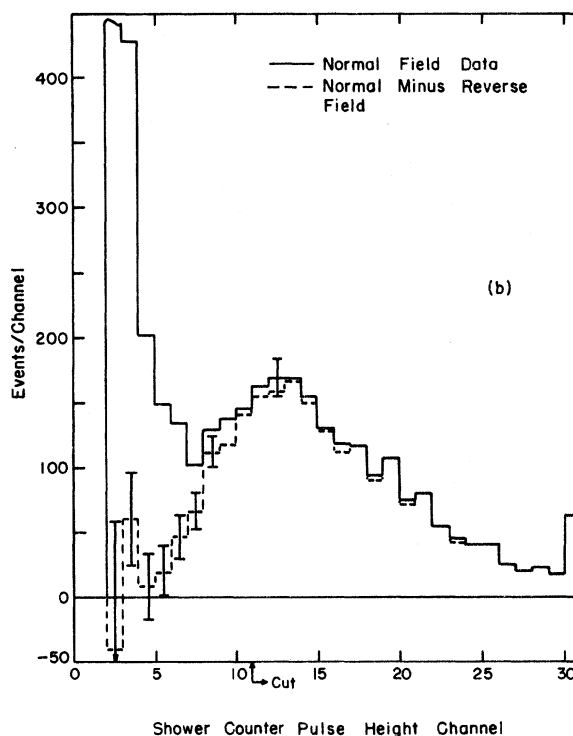

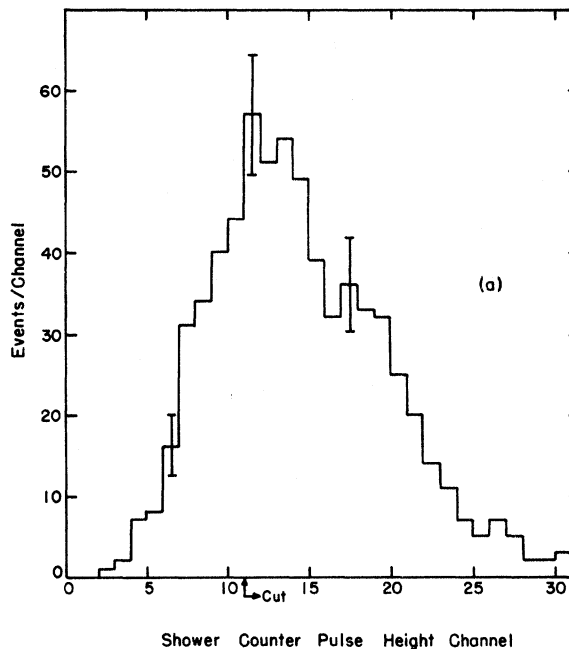FIG. 3. Shower-counter pulse-height spectrum at $q^2 = 29$ F^{-2}, $\theta = 90°$. (a) H_2 data with the analysis restricted to large Cherenkov counter pulse heights and to the peaks in the proton time-of-flight, and electron momentum distributions; (b) D_2 events with large Cherenkov counter pulse heights. The dashed line shows the same data after the subtraction of the reversed-field run data.

H_2 data are corrected for the empty-target background and the proton counter efficiency. The proton counter efficiency is determined from the data in the 4% momentum bite centered on the elastic momentum peak. The excess $e\bar{p}$ events amount to about 3% of the elastic e-p events, independent of q^2. They are not accounted for by the reverse-field measurements since the latter normally are less than 1% of the elastic e-p rates. It is found that, above the analysis cuts, the Cherenkov and shower counter spectra for the excess $e\bar{p}$'s are the same as for elastically scattered electrons. Thus it appears that these events are caused by high energy electrons. The momentum spectrum of the excess $e\bar{p}$'s is quite flat.

All of the above stated properties of the excess $e\bar{p}$ events are consistent with those expected from electron scattering from heavy nuclei. Indeed, a crust was observed to build up on the end caps of the target when it was refrigerated. The crust disappeared when the target was warmed up. Since the empty target runs were taken with the target warm, the contribution due to the crust would not be included in the empty target runs. The rate of build-up of the crust observed at the normal pressure of operation (10^{-6} torr) would increase the electron counting rate by roughly 0.2% per 8 h, assuming the density of the crust to be 1.0 g/cm^3. At this rate the contributions to the prime data runs due to the crust are calculated to be typically less than 1% and never more than 2%. Although the contributions from the observed excess $e\bar{p}$'s are somewhat larger than these estimates and do not tend to increase with refrigeration time, it is assumed that this background can be subtracted from the data using the shape of the empty-target data. Thus, the empty-target subtraction is increased enough to completely remove the excess $e\bar{p}$ events from the H_2 data. The effect of this is to essentially double the size of the empty-target subtraction. The empty-target subtraction from the D_2 data is similarly increased. The systematic error assigned to the reverse-field and extra empty-target subtractions is $\frac{1}{3}$ their size.

A further effect found in the H_2 data is a change in shape of the proton hodoscope distribution as the electron momentum is varied. The vertical proton distribution is used in order to avoid most of the effect of the radiative process on the proton direction. A large part of the correlation between the proton distribution and the measured electron momentum can be explained in terms of the dependence of the multiple scattering part of the momentum resolution function on the slope of the electron. Outside a momentum bite of 6% (centered on the elastic peak) and outside a proton vertical angle

region of $\pm 2°$ there remain unexplained events after empty-target and reverse-field run subtractions (0.4%) and random corrections (0.2%). These unexplained events amount to about 2% of the elastic e-p events at all q^2. Except for the correlation between the proton direction and the electron momentum these events are indistinguishable from elastic e-p events. For instance, their shower counter spectra and proton time-of-flight distributions are the same as those for elastic e-p events. It is concluded that these events are associated with the elastic e-p process (possibly outside the correct spectrometer acceptance) and that the effect is probably the same on D_2 as on H_2. Since the results presented here are given in terms of ratios of D_2 measurements to H_2 measurements, this effect should not change the results.

C. Corrections to Data

In this section we list the experimental corrections made to the data. Theoretical "corrections" are discussed in Sec. IV D. Throughout the analysis procedure, the data for each momentum bin are handled separately and the distinction between electron events with and without proton coincidences is maintained. The corrections are applied to the data obtained from the computer analysis in the following order:

(a) Cherenkov and shower counter efficiencies as discussed in Sec. IV A;

(b) correction for acceptable events whose momentum cannot be assigned by the computer (see Sec. IV A);

(c) normalization factors for each run to correct for small deviations from the nominal kinematical running conditions;

(d) accidentals correction to proton coincidence events as determined by a delayed coincidence technique. The randoms probability in the proton triple coincidence is typically 6%;

(e) background subtractions (Sec. IV B) including empty target, reverse field runs, extra empty target and hydrogen contamination in the deuterium;

(f) proton absorption and neutron conversion corrections. The proton absorption probability is calculated to be (3.0 ± 0.4)% (Ref. 1) essentially independent of q^2. This can be measured in the present experiment using the events in the elastic momentum peak in the H_2 data. The measured absorption probability is independent of q^2, the average over all q^2 being (2.2 ± 0.2)%. The experimentally determined values are used to make the corrections to the D_2 data. The neutron conversion probability is calculated to be (0.3 ± 0.1)% and is also fairly independent of q^2;

(g) normalization factors to convert the data to

cross sections. Among these factors is the electron solid angle, which is slightly different for each momentum bin, and a correction for the computer deadtime. For a more complete discussion of the normalization factors, see Ref. 2.

D. Theoretical Calculations

This section deals with the method used to compare theoretical cross sections with the measurements. The procedure on D_2 starts with the scattering cross section $d^2\sigma/d\Omega\,dE'$ predicted by a given theory evaluated with a reasonable set of form factors. The radiative corrections are applied to this spectrum using a δ-function technique described in Ref. 1; the deficiencies of the Meister and Griffy[19] formulism already noted in Ref. 1 should be reemphasized. The radiative correction function used in the δ-function technique is taken mainly from Mo and Tsai.[20] To include radiation from the proton lines, the Z and Z^2 terms of Meister and Yennie[21] are multiplied by $\sigma_p/(\sigma_p+\sigma_n)$ (since there is no radiation from the neutron lines) and added to the Mo and Tsai correction. The effect of the variation with energy of the elastic e-p matrix element is properly taken into account in Mo and Tsai's calculation. The physical radiators before and after scattering, 0.0028 and 0.0051 radiation lengths, respectively, are easily included in the Mo and Tsai calculation.

The effect of the experimental momentum resolution is included by folding the theoretical radiated spectrum with the resolution function. The resolution function is represented by the sum of two Gaussian distributions which enables the multiple scattering contribution to more closely follow the plural scattering tails of the distribution than does a single Gaussian.[22] Finally, the double-differential cross section measured by each momentum bin of the spectrometer is obtained by integrating the theoretical spectrum over the momentum bin and dividing by the bin width.

The theoretical momentum spectrum for those electrons which have a proton in coincidence is calculated by integrating $d^3\sigma/d\Omega\,dE'd\Omega_p^*$ over the proton counter aperture. The treatment of this spectrum is identical to that for the full electron spectrum described above. After the spectra are projected onto the momentum bins, the predicted value of the ratio $(ep)/e$ is calculated for each momentum bin.

The calculation of the H_2 momentum spectrum proceeds in a manner similar to that described above. The radiative correction differs slightly in that the full Z and Z^2 terms are used and the physical radiators before and after scattering are 0.0025 and 0.0048 radiation lengths, respectively. Since the radiative corrections are included in a

similar fashion for both D_2 and H_2, most uncertainties in the radiative corrections will cancel in taking the ratio of the D_2 cross sections to those from H_2.

In the present analysis it is possible to vary certain parameters which affect the results of the theoretical calculation in order to obtain the best fit to the measured momentum spectra. The parameters which may be varied are the over-all normalization of the cross section, the experimental resolution, the central momentum of the spectrometer, and the normalization of the N^* contribution. Only the width of the momentum-independent contribution to the resolution function is allowed to vary; the multiple scattering contribution is based on calculation. In practice, the H_2 data are used to determine the resolution and central momentum parameters. In obtaining the best fit to the D_2 spectra, these parameters are fixed while the normalizations of the quasielastic and the N^* spectra are varied.

V. EXPERIMENTAL RESULTS

In the following sections we describe the results obtained in the present experiment. In Secs. V A and V B we discuss the electron momentum spectra obtained on hydrogen and deuterium. The values of σ_n/σ_p determined from these spectra using the peak and area methods are presented in Secs. V C and V D. Section V E describes the results of two important tests of the deuteron theory in which the proton coincidence data on deuterium are used to predict σ_p. A third test of the theory is presented in Sec. V F. The values of σ_n/σ_p obtained through the proton coincidence method are given in Sec. V G.

A. Electron Momentum Spectra from H_2

The hydrogen data serve as a basic calibration of the apparatus. Besides providing measurements of the elastic e-p cross section σ_p, the hydrogen data determine several characteristics of the apparatus which are important in the analysis of the deuterium data: the momentum resolution of the electron spectrometer, the momentum scale of the spectrometer, and the efficiency of the proton detector.

Figure 4 shows a typical momentum spectrum of electrons scattered from H_2, this one at $q^2=29$ F^{-2}, $\theta=90\,°$. The theoretical histogram shown represents the best fit to the data obtained following the procedure described in Sec. IV D. The fits to the data at all q^2 are generally quite good. The measured H_2 momentum spectra drop essentially to zero above the elastic peak indicating that the background subtractions described in Sec. IV B are correct. The observed momentum distributions are found to have slightly more events in

their tails than predicted by the resolution function used in the fitting procedure. This difficulty arises because the resolution function employed does not properly include the long tails arising from plural or single scattering. Calculations show that the events with momentum greater than 1.04 E'_{peak}, approximately 2% of all events, are accounted for by plural scattering. The widths of the resolution functions found by the fitting procedure agree well with predictions.

The absolute values of σ_p obtained from the H_2 data, presented in Ref. 2, are in good agreement with previous measurements. It should be noted that the background subtractions are handled slightly differently in Ref. 2 than they are here. The unexplained correlation between the proton hodoscope distribution and the electron momentum (described in Sec. IV B) is believed to be an aspect of the acceptance of the electron spectrometer which is not included in the calculation of the electron solid angle. Thus a background subtraction of about 3% is made in Ref. 2 in evaluating the absolute values of σ_p. It is well established, however, that the events concerned do arise from the elastic e-p process. This effect should modify both the H_2 and D_2 data similarly and hence should not alter the ratio of D_2 to H_2 cross sections. Accordingly we make no such subtraction here.

B. Electron Momentum Spectra from D_2

The experimental double-differential cross sections obtained on deuterium are displayed in Fig. 5. The error bars on the experimental points are dominated by statistical uncertainties although
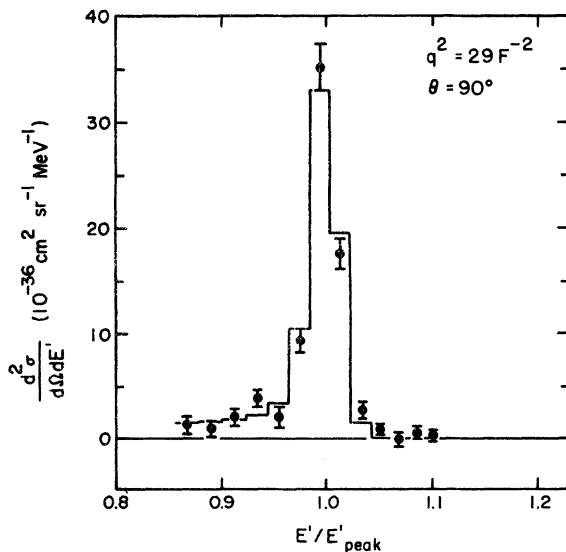

FIG. 4. Scattered electron momentum spectrum from hydrogen at $q^2 = 29$ F^{-2}, $\theta = 90°$.

they also include the 1.6% uncertainty in the relative momentum bin widths. The uncertainty in the over-all normalization, approximately 3%, is not included. The theoretical curves shown include the effects of the radiative corrections as well as the resolution of the spectrometer. The McGee theory shown here does not include FSI corrections. The theory of Renard *et al.* includes FSI corrections, although their meson-exchange term is excluded (see Sec. II). The theoretical curves are determined by allowing only the normalizations of the quasielastic and inelastic pion production spectra to vary separately to obtain the best fit to the data. The width of the resolution function and the momentum scale of the spectrometer are determined by the fits to the H_2 data.

It is observed that the theoretical curves fit the data quite well at all q^2. At low q^2 the data tend to follow the spectrum shapes predicted by the theory of Renard *et al.* somewhat better than those predicted by the McGee theory. This is particularly true in the region above $E' = 1.10$ E'_{peak} where FSI have their largest effect on the cross section. As q^2 increases, the difference between these two theories tends to diminish. The calculated shapes of the inelastic pion production (N^*) spectra (Sec. IV D) fit the data well. The factors by which the N^* spectra predicted by Adler's theory[18] are multiplied are 0.97 ± 0.05, 1.05 ± 0.09, and 1.50 ± 0.16 at $q^2 = 20$, 29, and 45 F^{-2}, respectively. These normalization factors are given relative to those for the quasielastic spectra to remove some of the dependence upon the proton and neutron form factors. Below $q^2 = 20$ F^{-2}, where the data do not include enough of the N^* region to allow determination of the normalization factors, they are taken to be unity.

C. σ_n/σ_p by Peak Method

The data near the peak of the quasielastic momentum spectra have been used to obtain $(\sigma_n + \sigma_p)/\sigma_p$ by the peak method. Since the resolution of the electron spectrometer is about one fourth as wide as the quasielastic peak, it is not possible to measure directly the cross section at the peak. In the present analysis, the cross section at the peak is inferred from the relation between the data in the three momentum bins nearest the peak and the theoretical prediction for the number of events in the corresponding momentum bite, $\Delta p/p = 6\%$. The results of the peak method analysis are given in Table II. The theoretical correction factors

$$\frac{d^2\sigma}{d\Omega\, dE'} \bigg/ (\sigma_n + \sigma_p)$$

are obtained from McGee's theory[4] without final state interactions. A -2.0% correction for FSI

effects is applied separately. The complete radi-
ative corrections to the measured peak cross sec-
tions are indicated in the Table. The effects of
the experimental resolution are included in the
calculation of the theoretical spectra. The approx-
imate size of the correction for these effects is
listed. The background subtractions are discussed
in Sec. IV B.

The net errors presented in Table II are ob-
tained by adding all sources of error in quadrature.
The statistical errors include those involved in
making the various background subtractions. The

remaining entries refer only to systematic errors.
The errors quoted for the momentum bite include
the uncertainty in the momentum width of the
three momentum bins used as well as the uncer-
tainty in the offset of the spectrum. The errors
in monitoring the beam between the D_2 and H_2 runs
include uncertainties in the following parameters:
beam position (which affects the electron scatter-
ing angle and solid angle), the incident beam en-
ergy, and the integrated beam intensity. The in-
crease in the beam monitoring error at low q^2
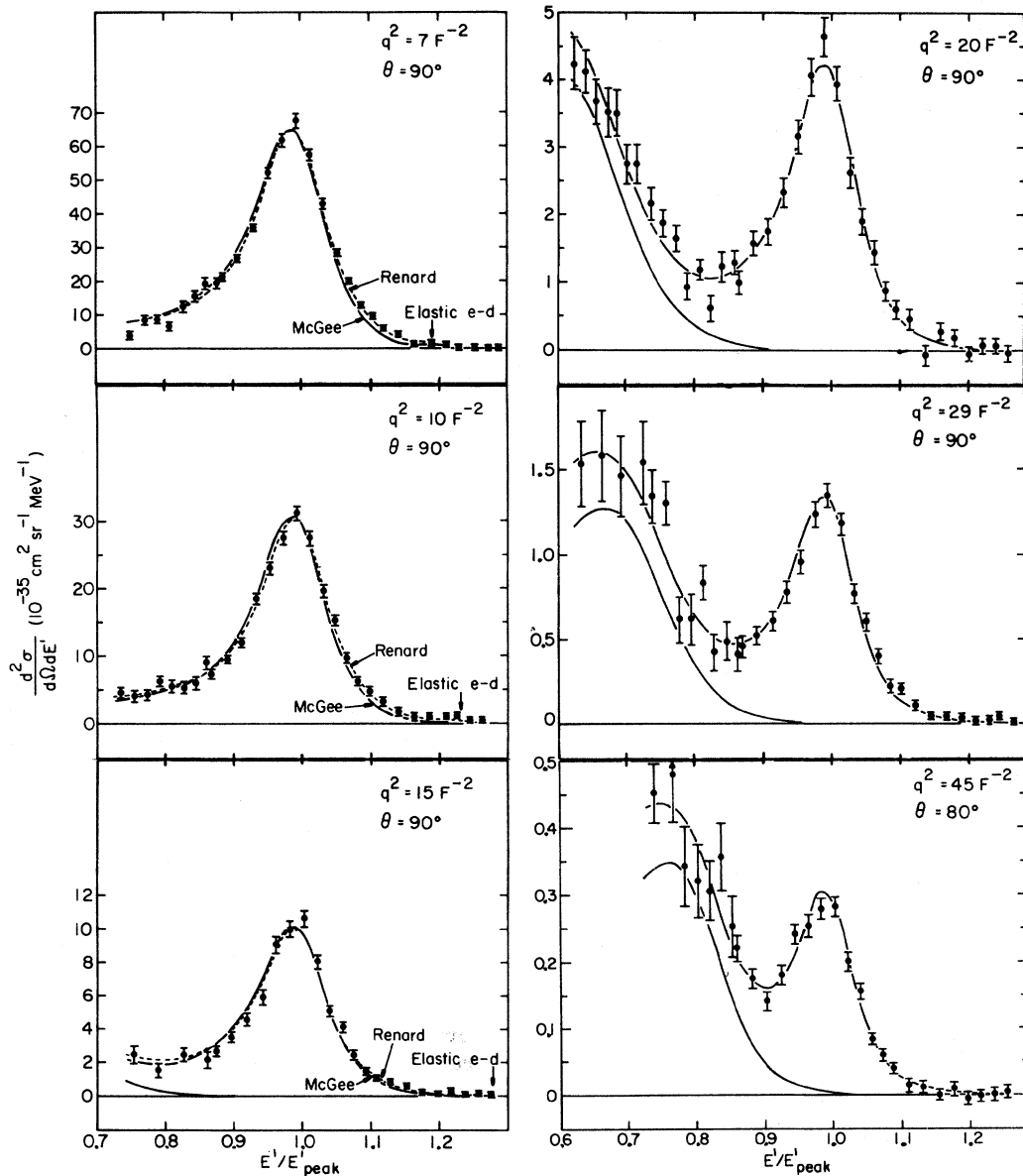reflects difficulties encountered in collecting the

FIG. 5. Scattered-electron momentum spectra from deuterium at all q^2. The theoretical curves are those predicted
by McGee (solid-lines) and Renard $et\ al.$ (dashed lines). The N^* contributions are shown separately.

TABLE II. $(\sigma_n + \sigma_p)/\sigma_p$: Peak method.

q^2 (F^{-2})	7.0	10.0	15.0	20.0	28.8	45.0
θ (deg)	90	90	90	90	90	80
$\dfrac{d^2\sigma}{d\Omega\,dE'}/\sigma_p$ (10^{-2} MeV^{-1}) (after all corr.)	3.13	2.87	2.46	2.26	2.20	1.74
$(\sigma_n + \sigma_p)/\sigma_p$	1.303	1.335	1.298	1.293	1.380	1.289
Theoretical corrections						
$\dfrac{d^2\sigma}{d\Omega\,dE'}/(\sigma_n + \sigma_p)$ (10^{-2} MeV^{-1})	2.457	2.188	1.936	1.785	1.624	1.348
FSI corrections	−2.0%	−2.0%	−2.0%	−2.0%	−2.0%	−2.0%
Rad. corr. factor	1.154	1.154	1.154	1.153	1.150	1.153
Exp. corr. to $d^2\sigma/d\Omega\,dE'$						
Resolution (% FWHM)	3.6	3.2	2.9	2.8	2.3	2.5
Corr. for resolution	−7.0%	−6.0%	−4.6%	−5.0%	−5.1%	−5.0%
Rev. field and extra ET subtraction	−2.9%	−3.7%	−2.5%	−4.0%	−3.6%	−8.0%
H_2 contamination subtraction	−0.3%	−0.2%	−0.2%	−0.2%	−0.2%	−0.2%
$N*$ subtraction	⋯	⋯	−0.01%	−0.05%	−0.3%	−1.9%
Corrections to σ_p						
Momentum bite:						
E'_{min}/E'_{peak}	0.872	0.857	0.864	0.857	0.881	0.917
E'_{max}/E'_{peak}	1.126	1.105	1.115	1.106	1.108	1.097
Rad. corr. factor (including resolution)	1.069	1.054	1.051	1.036	1.046	1.083
Rev. field and extra ET subtraction	−4.8%	−4.3%	−3.1%	−4.9%	−7.3%	−9.4%
Errors in $(\sigma_n + \sigma_p)/\sigma_p$						
Statistics	1.4%	2.1%	3.1%	5.3%	3.8%	5.5%
Momentum bite	2.6%	2.3%	2.0%	2.0%	2.0%	2.0%
Beam monitoring	3.0%	1.5%	1.0%	1.0%	1.0%	1.0%
Background subtractions	1.9%	1.9%	1.4%	2.1%	2.7%	4.1%
Resolution	2.0%	1.5%	1.0%	1.0%	1.0%	1.0%
Cherenkov and shower counter efficiencies	0.5%	0.6%	2.1%	1.9%	2.2%	3.0%
Net error	5.0%	4.2%	4.7%	6.5%	5.7%	7.9%

entire beam in the Faraday cup monitor at low energy. The corrections made to the H_2 data to obtain σ_p are also listed in Table II. The ratio of the molar densities of hydrogen to deuterium was taken to be 1.153.[23] Visual observation indicated that bubbling of the target liquid reduced the target density by less than 0.1%.

A comparison can be made between the peak method results obtained in the present experiment and those measured by Hughes *et al.*[13] at the same kinematical conditions. It is found that there is general agreement between the two experiments when the data of Hughes *et al.* are analyzed using the same theoretical corrections as are applied to the present measurements (see Sec. VI).

D. σ_n/σ_p by Area Method

The experimental objective in the area method is to measure the integral of the double-differential cross section over as much of the quasielastic spectrum as possible. The momentum region covered in the present experiment was extended

by taking supplementary data runs with the spectrometer's momentum bite shifted by ±15% relative to the peak position. The momentum intervals employed in the area method analysis are chosen to be as large as possible, consistent with keeping the necessary $N*$ subtractions reasonably small. Since the theoretical curves shown in Fig. 5 fit the experimental momentum distributions quite well, however, the area method results are insensitive to the choice of the lower momentum cutoff.

The area method results are presented in Table III along with an indication of the sizes of the corrections made to the data. The McGee theory without FSI corrections is used to determine $(\sigma_n + \sigma_p)/\sigma_p$ from the ratio of the area measured under the quasielastic e-d spectrum to the measured elastic e-p cross section σ_p. Most of the discussion of the background subtraction and errors involved in the peak method analysis apply equally well here. The 2.0% uncertainty in the full momentum bite of the spectrometer results in a 0.8% uncertainty in $(\sigma_n + \sigma_p)/\sigma_p$. This error is

TABLE III. $(\sigma_n + \sigma_p)/\sigma_p$:   Area method.

q^2 (F^{-2})	7.0	10.0	15.0	20.0	28.8	45.0
θ (deg)	90	90	90	90	90	80
Momentum bite:						
E'_{min}/E'_{peak}	0.789	0.785	0.793	0.785	0.787	0.847
E'_{max}/E'_{peak}	1.218	1.254	1.269	1.254	1.257	1.168
$(\sigma_n + \sigma_p)/\sigma_p$ (after all corr.)	1.271	1.357	1.251	1.226	1.329	1.324
Theoretical corrections						
Integrated $d^2\sigma/d\Omega\, dE'/(\sigma_n + \sigma_p)$	0.957	0.977	0.986	0.997	1.003	0.979
Rad. corr. factor	1.043	1.026	1.015	0.991	0.963	0.991
Exp. corr. to area						
Rev. field and extra ET subtraction	−4.6%	−4.6%	−3.2%	−6.6%	−7.8%	−11.1%
H_2 contamination subtraction	+0.2%	+0.2%	+0.2%	+0.2%	+0.2%	+0.2%
$N*$ subtraction	···	···	−0.6%	−2.6%	−10.4%	−15.3%
Elastic e-d subtraction	−0.55%	−0.13%	···	···	···	···
Errors in $(\sigma_n + \sigma_p)/\sigma_p$						
Statistics	1.3%	1.9%	2.9%	3.1%	3.9%	3.3%
Momentum bite	1.0%	0.9%	0.8%	0.8%	0.8%	0.8%
Beam monitoring	3.0%	1.5%	1.0%	1.0%	1.0%	1.0%
Background subtractions	2.2%	2.1%	1.5%	2.8%	4.1%	5.7%
Cherenkov and shower counter efficiencies	0.5%	0.6%	2.1%	1.9%	2.2%	3.0%
Net error	4.1%	3.4%	4.1%	4.8%	6.2%	7.3%

increased slightly at the lower q^2 to include increased uncertainties in the resolution function. The elastic e-d subtractions are based on previous measurements as discussed in Sec. IIIB.

E. σ_p from D_2 Coincidence Data

The coincidence taken between the large solid angle proton detector and the electron spectrometer in the present experiment not only allows the measurement of σ_n/σ_p by means of the proton coincidence method, but also provides three valuable tests of the validity of the quasielastic e-d theory. We first take up the discussion of two of these tests which involve the determination of σ_p from the electron-proton coincidence events, which we term the ep events, observed in the D_2 data. Such a determination is possible since the proton detector subtends most of the forward peak in the triple-differential cross section $d^3\sigma/ d\Omega\, dE'd\Omega_p^*$, which is primarily due to the e-p interaction (see Sec. II). Thus the electron momentum spectrum of the ep events is related to σ_p in much the same way as the momentum spectrum of all events is related to $\sigma_n + \sigma_p$. The D_2 coincidence momentum spectrum $(d^2\sigma/d\Omega\, dE')_{coin}$ is just the integral of the triple-differential cross section over the acceptance of the proton counter. In the present analysis, both the peak and area methods described in the foregoing sections are applied to the D_2 coincidence spectrum to obtain σ_p.

The values of the proton cross section obtained from the D_2 coincidence data, $(\sigma_p)_{D_2}$, relative to those measured directly on H_2, σ_p, are presented in Tables IV and V. The discussion of the corrections and errors given in Secs. VC and VD apply equally well to these results. The additional errors in the proton counter efficiencies and corrections for accidental coincidences have a negligible contribution to these results and have not been listed. The theoretical corrections used here are obtained from the McGee theory without any corrections for final-state-interaction effects in order to compare the present results directly with those obtained at $\theta = 20°$ by Budnitz et al.[1] This comparison is shown in Fig. 6. The Budnitz data have been reduced by 1.0% to correspond to the same deuteron wave function used in the present analysis. Also shown in Fig. 6 are the low q^2 points at $\theta = 20°$ presented in Appendix B. The present area-method results at 90° are consistent with the 20° results within their somewhat larger error bars. Both sets of data suggest that the ratio of the proton cross section derived from the D_2 measurements, $(\sigma_p)_{D_2}$, to that measured on H_2 is independent of q^2. The weighted average of $(\sigma_p)_{D_2}/\sigma_p$ from $q^2 = 7$ to 45 F^{-2} is 0.944 ± 0.020 at 90° and 0.926 ± 0.005 at 20° using the area method. The average of the peak method results at $\theta = 90°$ is 0.966 ± 0.024.

The determination of σ_p through the use of the

TABLE IV. $(\sigma_p)_{D_2}$: Peak method applied to D_2 coincidence data. No FSI corrections have been made.

q^2 (F^{-2})	7.0	10.0	15.0	20.0	28.8	45.0
θ (deg)	90	90	90	90	90	80
$\left(\dfrac{d^2\sigma}{d\Omega\,dE'}\right)_{coin}\Big/\sigma_p$ (after all corr.) (10^{-2} MeV^{-1})	2.42	2.14	1.91	1.71	1.53	1.12
$(\sigma_p)_{D_2}/\sigma_p$	0.995	0.983	0.990	0.959	0.955	0.848

Theoretical corrections

$\left(\dfrac{d^2\sigma}{d\Omega\,dE'}\right)_{coin}\Big/\sigma_p$ (10^{-2} MeV^{-1})	2.420	2.180	1.927	1.778	1.601	1.323
Rad. corr. factor	1.154	1.154	1.154	1.153	1.150	1.153

Exp. corr. to $(d^2\sigma/d\Omega\,dE')_{coin}$

Corr. for resolution	−7.0%	−6.0%	−4.6%	−5.0%	−5.1%	−5.0%
Rev. field and extra ET subtraction	−2.2%	−3.0%	−2.2%	−3.1%	−2.7%	−6.3%
H_2 contamination subtraction	−0.7%	−0.5%	−0.5%	−0.5%	−0.5%	−0.5%
$N*$ subtraction	···	···	···	−0.02%	−0.02%	−0.5%

Errors in $(\sigma_p)_{D_2}/\sigma_p$

Statistics	1.6%	2.3%	7.3%	4.6%	5.5%	7.8%
Momentum bite	2.6%	2.3%	2.0%	2.0%	2.0%	2.0%
Beam monitoring	3.0%	1.5%	1.0%	1.0%	1.0%	1.0%
Background subtractions	1.8%	1.7%	1.3%	1.9%	2.6%	3.8%
Resolution	2.0%	1.5%	1.0%	1.0%	1.0%	1.0%
Cherenkov and shower counter efficiencies	0.5%	0.6%	2.1%	1.9%	2.2%	3.0%
Net error	5.1%	4.3%	8.1%	5.9%	6.9%	9.5%

TABLE V. $(\sigma_p)_{D_2}$: Area method applied to D_2 coincidence data. No FSI corrections have been made.

q^2 (F^{-2})	7.0	10.0	15.0	20.0	28.8	45.0
θ (deg)	90	90	90	90	90	80

Momentum bite:

E'_{min}/E'_{peak}	0.798	0.785	0.862	0.857	0.787	0.851
E'_{max}/E'_{peak}	1.218	1.254	1.112	1.106	1.257	1.097
$(\sigma_p)_{D_2}/\sigma_p$ (after all corr.)	0.968	0.974	0.942	0.909	0.924	0.862

Theoretical corrections

Integrated $(d^2\sigma/d\Omega\,dE')_{coin}/\sigma_p$	0.930	0.963	0.915	0.960	0.967	0.921
Rad. corr. factor	1.043	1.026	1.060	1.094	0.963	0.995

Exp. corr. to area

Rev. field and extra ET subtraction	−3.0%	−3.3%	−2.6%	−7.6%	−4.9%	−7.6%
H_2 contamination subtraction	0%	0%	0%	0%	0%	0%
$N*$ subtraction	···	···	−0.04%	−0.25%	−0.8%	−4.9%
Elastic e-d subtraction	0.70%	0.18%	···	···	···	···

Errors in $(\sigma_p)_{D_2}/\sigma_p$

Statistics	1.4%	2.0%	6.0%	3.5%	4.9%	6.1%
Momentum bite	1.0%	0.9%	0.8%	0.8%	0.8%	0.8%
Beam monitoring	3.0%	1.5%	1.0%	1.0%	1.0%	1.0%
Background subtractions	1.9%	1.8%	1.4%	3.0%	2.9%	4.0%
Cherenkov and shower counter efficiencies	0.5%	0.6%	2.1%	1.9%	2.2%	3.0%
Net error	4.0%	3.3%	6.6%	5.1%	6.2%	8.0%

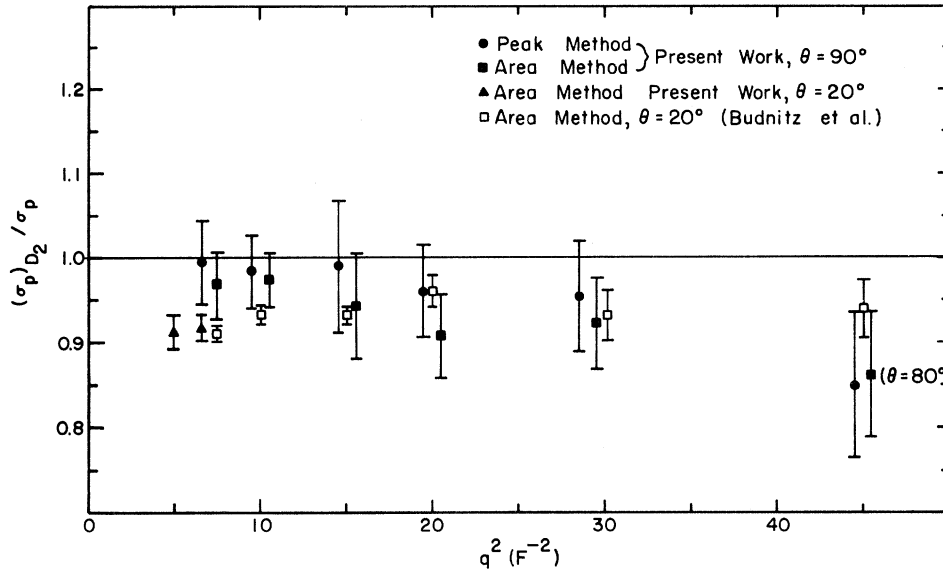FIG. 6. σ_p derived from proton coincidence measurements on deuterium.

proton coincidence data involves two distinct aspects of the quasielastic $e\text{-}d$ theory: (a) the normalization of the double-differential cross section, and (b) the proper prediction of f_p, the fraction of events which have a proton in coincidence with the detected electron. It is thought that the failure of the McGee theory to explain the above proton coincidence results is due, in large part, to the omission of the FSI effects in the present calculations. For example, the -2.0% correction applied to the peak cross sections to take account of FSI would have the effect of increasing $(\sigma_p)_{D_2}$ by 2.0%. Furthermore, $(\sigma_p)_{D_2}$ would be increased by an additional 2% due to the effect of FSI on f_p at the quasielastic peak if the difference between the values of f_p predicted by McGee and Renard et $al.$ (with FSI) is taken to be a measure of this effect. The combination of these two corrections for FSI brings the values of $(\sigma_p)_{D_2}$ for the peak method into line with σ_p measured directly on hydrogen.

It is interesting to note the effect on the above proton coincidence results of using the theory of Renard et $al.$ to analyze the data. Above $q^2 = 7$ F^{-2} the use of this theory, without the meson-exchange term, would increase the ratios $(\sigma_p)_{D_2}/\sigma_p$ obtained by both the peak and area methods by about 3% at both $20°$ and $90°$, while for $q^2 = 7$ F^{-2} and below, the increase would be slightly larger. Thus, the use of this theory would bring the ratios closer to unity, although the more accurate $20°$ results would still be significantly too low by about 3%. It was pointed out in Sec. II that the normalization of the cross sections predicted by the theory of Renard et $al.$ is in question. The normalization discrepancy found between their theory and that

of McGee is about 3% and is in such a direction as to improve the agreement between $(\sigma_p)_{D_2}$ and σ_p if their normalization were brought into line with McGee's. We note in passing that the inclusion of the meson-exchange term would decrease the ratios by about 1% from those obtained with the McGee theory.

F. Variation of f_p with E'

We now turn our attention to the third test of the quasielastic $e\text{-}d$ theory afforded by the proton coincidence data. In this test the theory is asked to properly predict the variation of f_p as a function of E', as first seen by Budnitz et $al.$[1] (f_p is the fraction of the electron events which possess a proton in coincidence with the electron.) Figure 7 shows the experimentally observed dependence of f_p upon E' at $q^2 = 7$ and 10 F^{-2}, $\theta = 90°$. At the higher q^2 points the data are inadequate to show this dependence. The data points shown in Fig. 7 include accidental corrections, background subtractions, and corrections for the proton counter efficiency and neutron conversion probability. The error bars are dominated by statistical uncertainties. The variation of f_p with E' depicted in Fig. 7 is not as dramatic as that observed at $\theta = 20°$ (see Appendix B), partly due to the poor statistical accuracy of the data in the momentum regions away from the quasielastic peak. Consequently, much of the following discussion will be based on the more accurate results obtained at $\theta = 20°$.

The theoretical curves displayed in Fig. 7 have been calculated for the present experimental situation and may be compared directly with the experimental results. These curves have been scaled

to match the experimental values of f_p in the region of the quasielastic peak designated by the brackets in the figure. This renormalization of the curves corresponds to a change in the value of σ_n used in the theoretical calculation and is the basis of the proton coincidence method for determining $(\sigma_n + \sigma_p)/\sigma_p$. It is observed that the McGee theory without FSI does not predict the experimentally observed dependence of f_p upon E'. It was also found that the use of the McGee theory led to incorrect values of $(\sigma_p)_{D_2}$. It is unlikely, therefore, that the McGee theory can be relied upon to interpret the proton coincidence data in terms of $(\sigma_n + \sigma_p)/\sigma_p$. On the other hand, the theory of Renard *et al.*, including FSI, appears to fit the observed variation of f_p with E' quite well. It was also found to predict values of $(\sigma_p)_{D_2}/\sigma_p$ which are closer to unity than those obtained through the use of the McGee theory, although the absolute normalization of its cross sections is questionable. It should be noted, however, that f_p involves the ratio of cross sections and does not depend upon the over-all normalization of the cross sections. What is important here is that the theory properly predict the *shape* of the proton distribution in the c.m. of the final neutron-proton system (see Fig. 1). It appears, therefore, that the theory of Renard *et al.* may be adequate to interpret to measured values of f_p in terms of $(\sigma_n + \sigma_p)/\sigma_p$, i.e., it may be used in the proton coincidence method.

In order to allow the comparison of future theoretical calculations with the results of the present experiment, the effective cone angles subtended by the proton counters at $q^2 = 7$ and 10 F^{-2} are listed in Table VI as a function of E'. If a theoretical calculation of the fraction f_p is carried out using the effective laboratory angles, the result will be very nearly the same as that obtained

TABLE VI. Effective ω_{lab} subtended by proton counters for $\theta = 90°$.

	Effective ω_{lab} (deg)	
$E'/E'_{H_2\,peak}$	$q^2 = 7$ F^{-2}	10 F^{-2}
1.18	$\cdots$	20.08
1.15	18.79	20.21
1.12	20.57	20.33
1.09	20.64	20.47
1.06	20.64	20.60
1.03	20.52	20.55
1.00	20.55	20.65
0.97	20.32	20.59
0.94	20.21	20.34
0.91	20.07	20.32
0.88	19.81	20.20
0.85	19.53	19.98
0.82	19.29	19.65
0.79	18.96	19.40
0.76	18.55	19.05

from a complete calculation including the details of the experimental setup. These effective angles *do not include*, however, the effects of the momentum resolution and radiative corrections which must be included separately for an accurate comparison with the data. The effective cone angles for the momentum bites used in obtaining the proton coincidence method results are 19.3°, 16.5°, 9.43°, and 6.73° at $q^2 = 15$, 20, 28.8, and 45 F^{-2}, respectively.
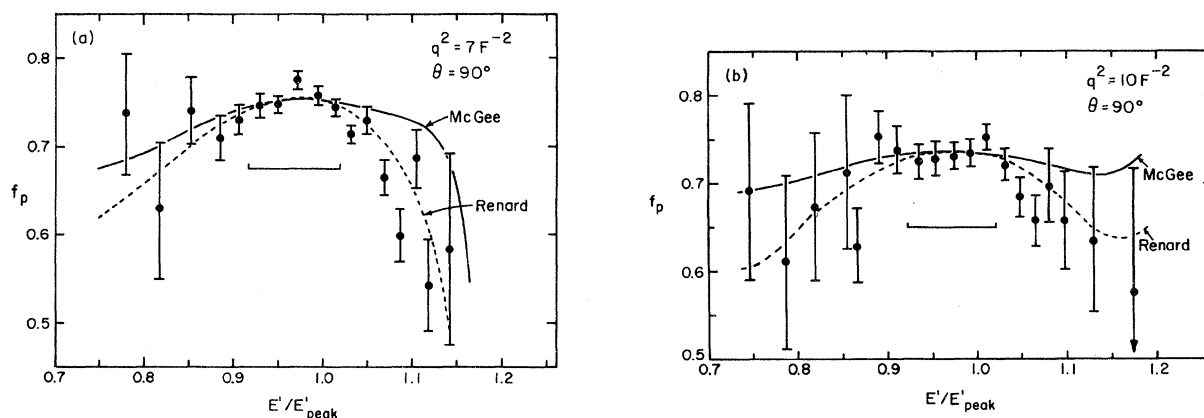

FIG. 7. f_p, the fraction of events with a proton coincidence, vs E' (a) at $q^2 = 7$ F^{-2} and (b) at $q^2 = 10$ F^{-2}; both for $\theta = 90°$. The theoretical predictions of McGee and of Renard *et al.* are shown. The brackets indicate the momentum bite used in the proton coincidence method.

TABLE VII. $(\sigma_n + \sigma_p)/\sigma_p$: Proton coincidence method.

q^2 (F^{-2})		7.0	10.0	15.0	20.0	28.8	45.0
θ (deg)		90	90	90	90	90	80
Momentum bite:							
E'_{min}/E'_{peak}		0.921	0.924	0.931	0.924	0.926	0.958
E'_{max}/E'_{peak}		1.024	1.023	1.031	1.024	1.025	1.033
$(\sigma_n + \sigma_p)/\sigma_p$ (after all corr.):	McGee	1.302	1.351	1.300	1.321	1.406	1.400
	Renard	1.264	1.318	1.271	1.291	1.374	1.368
Theoretical corrections							
Corr. factor to f_p :	McGee	1.016	1.007	1.004	1.003	1.017	1.020
	Renard	1.047	1.031	1.027	1.026	1.040	1.043
Exp. corrections							
Randoms prob.		5.8%	5.4%	6.1%	6.1%	5.2%	6.9%
Proton counter inefficiency		2.0%	1.8%	1.9%	2.0%	2.4%	2.7%
Neutron conversion prob.		0.3%	'0.3%	0.3%	0.3%	0.3%	0.3%
Effect on $(\sigma_n + \sigma_p)/\sigma_p$ of subtractions:							
Ref. field and extra ET subtraction		+0.5%	−1.0%	+1.2%	+2.2%	+0.2%	−1.4%
H_2 contamination subtraction		+0.2%	+0.2%	+0.2%	+0.2%	+0.2%	+0.2%
N^* subtraction		...	...	...	−0.1%	−0.5%	−1.2%
Errors in $(\sigma_n + \sigma_p)/\sigma_p$							
Statistics		0.7%	1.0%	2.9%	2.0%	2.1%	3.6%
Background subtractions		1.2%	1.6%	1.1%	1.7%	1.5%	3.4%
Proton counter efficiency		0.3%	0.6%	0.7%	1.0%	1.3%	1.3%
Randoms corr.		0.6%	0.5%	0.6%	0.6%	0.5%	0.7%
Net error		1.4%	2.0%	3.2%	2.8%	2.9%	5.1%

G. σ_n/σ_p by Proton Coincidence Method

The values of $(\sigma_n + \sigma_p)/\sigma_p$ obtained by the proton coincidence method using the values of f_p measured near the quasielastic peak are listed in Table VII. The results are quoted using the theories of both McGee and Renard et al. to interpret the data. Above $q^2 = 15$ F^{-2} the correction factor of Renard et al. is taken to be a constant 2.3% larger than the McGee factor, as observed at $q^2 = 10$ and 15 F^{-2}. This is reasonable since the effects of FSI are thought to be fairly constant above $q^2 = 10$ F^{-2}. Also, it is found that the correction factors are somewhat independent of ω^*, the c.m. polar angle of the outgoing proton.

The experimental corrections listed in Table VII have been discussed in Sec. IV. The statistical errors listed include the statistical uncertainties in the background subtractions and in the determination of the randoms probability. The systematic uncertainties in the background, which are listed separately, are found by assuming an independent error in both the electron-proton coincidence and anticoincidence background contributions equal to $\frac{1}{3}$ their magnitude. The errors in the proton counter efficiencies arise from the statistical uncertainties in the H_2 from which they are deter-

mined. The systematic uncertainty in the correction for accidental coincidences is taken to be $\frac{1}{10}$ the randoms probability.

A comparison between the values of σ_n/σ_p obtained by the three different methods employed in the present experiment is shown in Fig. 8. The error bars shown are the full errors quoted in Tables II, III, and VII. These error bars are somewhat larger than appropriate for a comparison between the different methods since there is a correlation between the uncertainties ascribed to each method. This correlation is most evident between the peak and area methods as the peak method makes use of a subset of the deuterium data employed in the area method. Furthermore, in both methods, the D_2 cross sections are normalized to the same H_2 cross sections. These comments aside, there is good agreement between the values of $(\sigma_n + \sigma_p)/\sigma_p$ obtained by the different methods on the 4% level. This agreement indicates that the theoretical treatments applied to the three methods used here are consistent with each other. This conclusion is strengthened by the 20° results presented in Appendix B since when the same theoretical treatment is used to analyze the 20° data, the values of $(\sigma_n + \sigma_p)/\sigma_p$ obtained by the area and proton coincidence methods agree within 2% error bars.
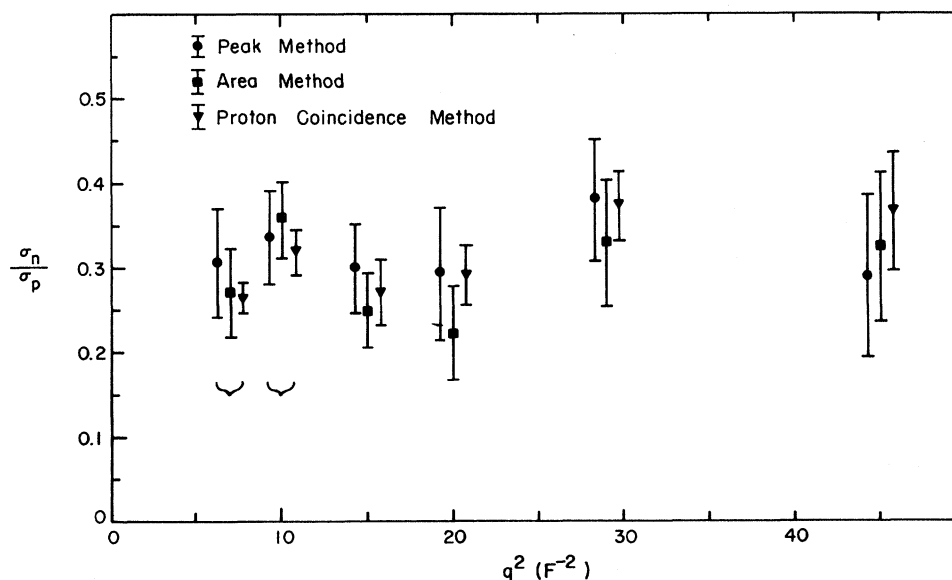
FIG. 8. σ_n/σ_p results for the three methods employed in the present experiment.

VI. NEUTRON FORM FACTORS

Figure 9 shows a comparison between the values of σ_n/σ_p obtained here and those obtained from previous quasielastic e-d measurements at $q^2 = 10$ and 30 F^{-2}. In order to provide a consistent basis of interpretation for the present comparison, as well as for the determination of the neutron form factors, the results from previous experiments have been analyzed using the theoretical treatment described in the present work. The measurements considered and the corrections applied to them are the following:

(a) Budnitz *et al.*[1] have made measurements using the area and proton coincidence methods. Their values of $(\sigma_n + \sigma_p)/\sigma_p$ from the area method have been multiplied by 0.990 to correspond to the slightly different deuteron wave functions used in the present work (see Sec. IIA), and those obtained by the proton coincidence method have been multiplied by 0.977 above $q^2 = 7$ F^{-2} to conform to the corrections given by the theory of Renard *et al.* (at $q^2 = 7$ F^{-2} the correction factor is 0.972).

(b) Bartel *et al.*[24, 25] have employed the neutron-proton coincidence method which should be insensitive to FSI effects. Indeed, the theory of Renard *et al.* predicts the correction to σ_n/σ_p to be less than 1%. No corrections have been made to these data.

(c) Stein *et al.*[26] also used the neutron-proton coincidence method but quote a fairly large systematic error common to all points (9%). In order to reduce this over-all normalization error, their values of σ_n/σ_p have been reduced by 5% to bring

their results at $q^2 = 14.5$ F^{-2}, $\theta = 35°$ more into line with Bartel's result and their systematic error has been reduced to 7%.

(d) Albrecht *et al.*[27] have made peak method measurements at high q^2 mostly at $\theta = 48°$. Their correction factors to obtain $(\sigma_n + \sigma_p)/\sigma_p$ are only 0.6% higher than our theoretical treatment would predict. No corrections have been applied to their results.

(e) Galster *et al.*[28] have used the proton coincidence method using the McGee theory without FSI. Their values of $(\sigma_n + \sigma_p)/\sigma_p$ have been reduced by 2% to convert to the theory of Renard *et al.*

(f) Hughes *et al.*[13] have made extensive low-q^2 measurements using the peak method. Their values of $(\sigma_n + \sigma_p)/\sigma_p$ have been reduced by about 5% to correspond to the theoretical corrections applied to our peak-method results. This rather large correction may be accounted for as follows: Hughes *et al.* start with Durand's expression [Eq. (84), Ref. 7] for peak cross section, which is already 2% below ours (chiefly due to a difference in the triplet effective range assumed). To change to D-state probability of 7% from Durand's 5%, Hughes *et al.* reduce the cross section by 2% (twice as much as such a change in P_D actually produces in the peak cross section). Finally, they reduce the cross section by about 1% to include the effect of final-state interactions (already included in Durand's expression).

(g) Akerlof *et al.*[29] made measurements of peak cross sections at large angles. Since their error bars are much larger than the few percent difference between their theoretical corrections and

ours, no corrections have been made to their data.

From the present work, only the results obtained by the proton coincidence and area methods are included in the present analysis in order to avoid giving them undue weight. Also included at 7 F^{-2}, $\theta = 20°$ are the results presented in Appendix B which are in essential agreement with the measurements made by Budnitz *et al.*[1]

The values of σ_n/σ_p obtained here are found to be in general agreement with those obtained in previous experiments, although they tend to be slightly lower. It is interesting to note the excellent agreement between the area method results of Budnitz *et al.* at $\theta = 20°$ and those of Bartel *et al.* at $\theta = 10°$ for $q^2 = 10$, 15, and 20 F^{-2}. Bartel *et al.* used the neutron-proton coincidence method, which stands
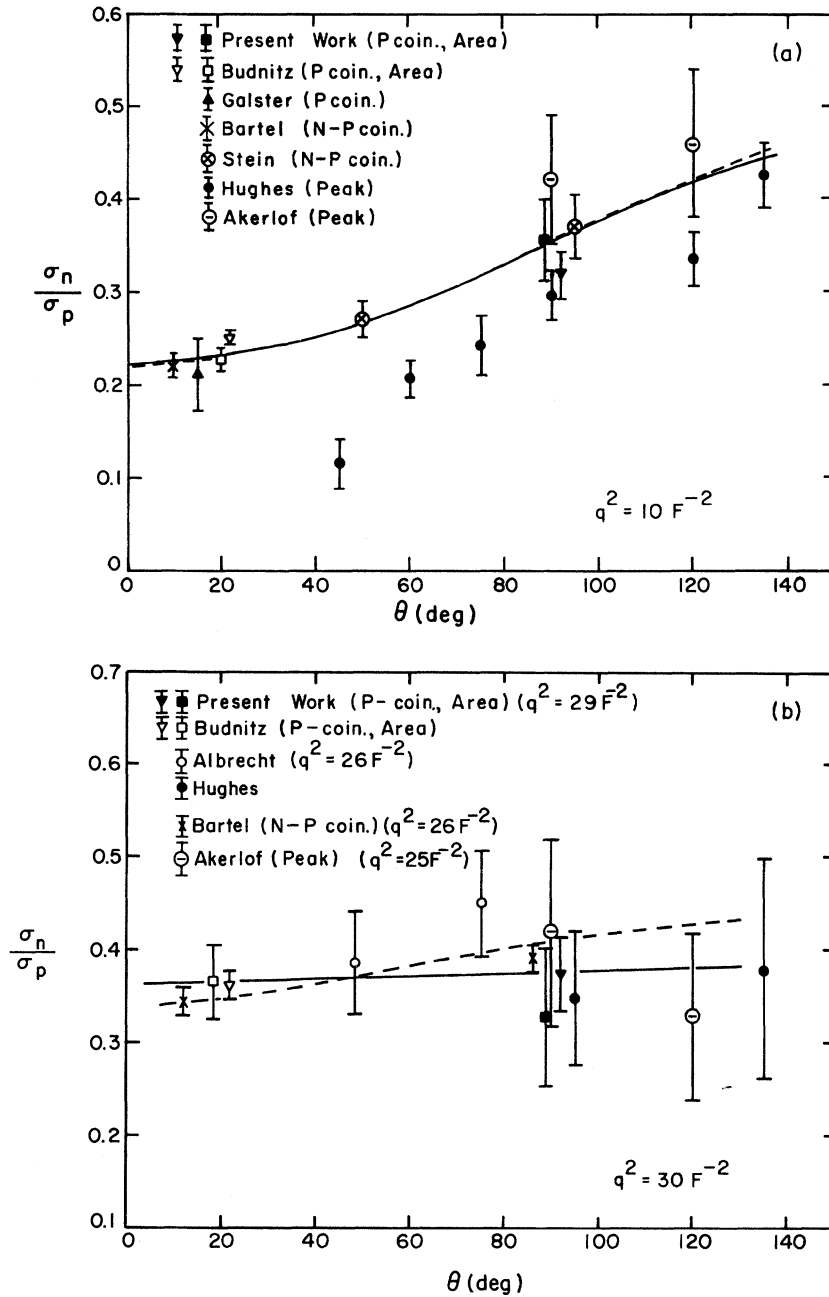

FIG. 9. Comparison of the present results with previous measurements (a) at $q^2 = 10$ F^{-2} and (b) at $q^2 = 30$ F^{-2}. The curves represent the best fits to the data as described in the text. The dashed line shows the effect of assuming $G_{En} = 0$.

TABLE VIII. Neutron form factors.

q^2 (F^{-2})	G_{Mp}	G_{Ep}	$\mu_p G_{Mn}/\mu_n G_{Mp}$	G_{En}^2
7.0	1.408 ± 1.1%	0.5004 ± 1.4%	0.9048 ± 0.0594	0.0132 ± 0.0090
10.0	1.1336 ± 0.9%	0.4147 ± 1.2%	1.0155 ± 0.0275	0.0010 ± 0.0045
15.0	0.8427 ± 0.6%	0.2926 ± 1.4%	0.9367 ± 0.0579	0.0028 ± 0.0072
20.0	0.6477 ± 1.0%	0.2174 ± 3.0%	0.7709 ± 0.0569	0.0212 ± 0.0046
30.0	0.4202 ± 0.8%	0.1307 ± 3.6%	0.9053 ± 0.0414	0.0052 ± 0.0028
45.0	0.2480 ± 1.1%	0.071 23 ± 9.0%	0.9353 ± 0.0708	0.0017 ± 0.0024

on a firmer theoretical basis than the other methods. The proton coincidence results of Budnitz *et al.* are also in fair agreement with the measurements of Bartel *et al.*, but tend to lie above them at the low-q^2 points. This agreement at small θ lends confidence to the area and proton coincidence methods which have been used in the present work.

The values of σ_n/σ_p obtained from the measurements of Hughes *et al.* decrease as θ approaches zero much more rapidly than those obtained by various other authors. It is for this reason that their form factor analysis consistently yielded negative values of G_{En}^2. Although the results of Hughes *et al.* only exhibit this disturbing discrepancy with the more recent measurements for θ less than 90° and at small q^2, all of their results have been ignored in the present form-factor analysis. We can offer no explanation for the observed discrepancies.

The neutron form factors G_{Mn} and G_{En} have been determined from the available quasielastic e-d measurements. The form factors are determined from the elastic e-n scattering sections σ_n by fitting the measured angular dependence of σ_n at fixed q^2 to the Rosenbluth formula[10] using a least-squares fitting procedure. For this purpose the σ_n/σ_p ratios are multiplied by the values of σ_p implied by the recent compilation of the proton form factors made by Price *et al.*[2] All of the quasielastic e-d measurements mentioned above

are included in the fitting procedure with the exception of the data presented by Hughes *et al.* (for the reasons already stated). The recent measurements of Bartel *et al.*[25] at high q^2 also are not included in the present analysis since they stand on their own. Instead, we use their form factors as a basis of comparison with the present results. In order to avoid giving the proton coincidence method data undue weight, an estimated 1.5% theoretical error in $(\sigma_n + \sigma_p)/\sigma_p$ is added in quadrature with the generally small experimental errors. No theoretical uncertainty is included in the results obtained by other methods since the experimental uncertainties are generally somewhat larger than the theoretical uncertainties involved.

The neutron form factors obtained are listed in Table VIII and are plotted versus q^2 in Figs. 10 and 11. The present results are seen to be in good agreement with those of Bartel *et al.*, which are plotted separately. The values of G_{Mn} obtained lie slightly below the so-called "scaling law,"

$$G_{Mn}(q^2)/\mu_n = G_{Mp}(q^2)/\mu_p . \qquad (3)$$

The scaling law holds at $q^2 = 0$ simply because of the way the form factors are defined. Whether or not the scaling law holds for nonzero values of q^2
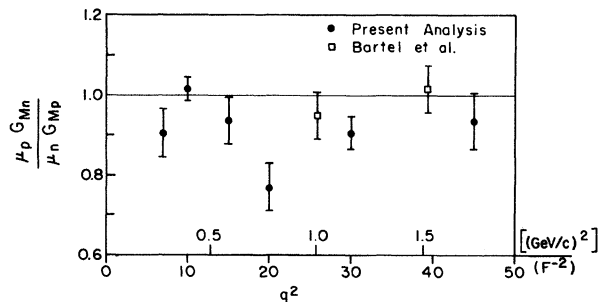

FIG. 10. The values of $\mu_p G_{Mn}/\mu_n G_{Mp}$ obtained from the best fits to the data as described in the text. The recent results of Bartel *et al.* are shown separately (squares).
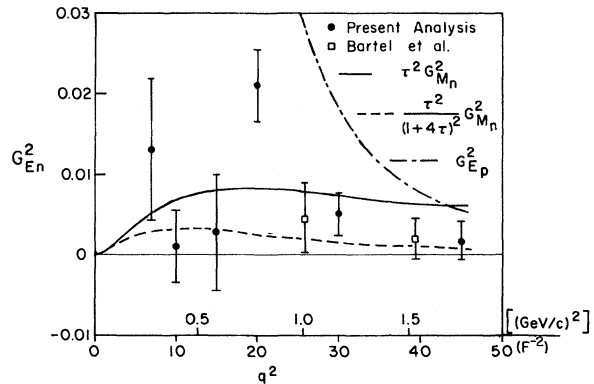

FIG. 11. The values of G_{En}^2 obtained from the best fits. The curves provide comparison with other form factors.

is, however, an experimental question. The data indicate that there may be small deviations from the scaling law, but not as large as the deviations observed in the corresponding "scaling law" for the proton form factors,[2]

$$G_{Mp}(q^2)/\mu_p = G_{Ep}(q^2) . \tag{4}$$

The values of G_{En}^2 obtained in the present analysis are positive at all q^2. This is in contrast to most previous analyses[1,13,24,26] of quasielastic e-d data which have obtained negative values of G_{En}^2, which is, of course, physically untenable. The usual approach in these cases has been to set $G_{En} = 0$. It is known from experiments involving the scattering of thermal neutrons from noble gases, however, that although $G_{En} = 0$ at $q^2 = 0$, G_{En} has a positive slope there.[30] Furthermore, when the relativistic corrections of Casper and Gross[31] are applied to elastic e-d scattering measurements,[32] the values of G_{En} obtained below $q^2 = 3$ F^{-2} are consistent with the thermal neutron measurement of the slope at $q^2 = 0$. It seems unlikely, therefore, that G_{En} is truly equal to zero in the moderate range of q^2 covered in the present experiment. What must be answered *experimentally* is: How small is G_{En}?

In the quasielastic e-d experiments used in the present analysis, it is G_{En}^2 which is linearly related to the experimental quantities, not G_{En}. Therefore the error bars drawn in Fig. 11 are related to a normal error distribution in the usual manner. If we omit the anomalously high point at $q^2 = 20$ F^{-2}, the remaining data points are insufficient to conclude definitely that $G_{En} \neq 0$, although there is some tendency to indicate this. The data are consistent with either of the following relations which have roughly the proper slope at $q^2 = 0$: $G_{En} = -\tau G_{Mn}$ or $G_{En} = [-\tau/(1 + 4\tau)] G_{Mn}$ (suggested by Budnitz et al.[1]), where $\tau = q^2/4M_p^2$. The latter expression, which is slightly preferred by the present results, is reasonably consistent with the elastic e-d results.[32]

The variation of σ_n/σ_p with θ implied by the presently obtained neutron form factors at $q^2 = 10$ and 30 F^{-2} is shown in Fig. 9. It is interesting to observe the effect of setting $G_{En} = 0$ on the variation of σ_n/σ_p. The curves which result when G_{En} is assumed to be zero, i.e., G_{Mn} is the only variable in fitting procedure, are shown in Fig. 9. There is only a small change in the curves when G_{En} is set equal to zero. This is the reason it is difficult to measure G_{En}. It is observed that no single measurement of σ_n/σ_p made at large θ has sufficient accuracy to distinguish between zero and nonzero values of G_{En}^2, with the possible exception of the recent results of Bartel et al.[25]

VII. CONCLUSIONS

It has been shown that the theory of Renard *et al.*, which includes the effects of final state interactions (FSI), satisfactorily predicts certain aspects of the behavior of the proton coincidence data, whereas the theory of McGee without FSI does not. However, the normalization of the cross sections given by their theory as well as the validity of some of their additional small terms, notably the meson-exchange terms, are in question. Thus, while the theory of Renard *et al.* may be used in the proton coincidence method analysis to obtain σ_n/σ_p, it probably should not be used in the peak or area method analyses. For the latter two methods, which involve measurements of the electron only, it seems reasonable to use McGee's theory along with corrections for the effects of FSI. Further theoretical calculations are to be encouraged in order to resolve the discrepancies between these two theories.

Form factor fits to the existing quasielastic electron-deuteron data have resulted in values for G_{Mn} which are slightly below the "scaling law" relation and generally positive values of G_{En}^2. The existing data tend to indicate that $G_{En} \neq 0$, although not conclusively. It is apparent that in order to conclusively show G_{En} is nonzero through quasielastic e-d measurements, further experiments with even better precision than that obtained recently by Bartel et al. (about 5% in σ_n/σ_p) will be needed. This is true at all q^2 and for all θ. To avoid significant theoretical uncertainties, such experiments should employ the neutron-proton coincidence method.

ACKNOWLEDGMENTS

APPENDIX A: SOME ANALYTIC FORMULAS

The modified Hulthén model for the deuteron wave functions used in the present evaluation of the McGee theory has the form:

S state: $u(r) = N\cos\epsilon(e^{-\alpha r} - e^{-\beta r})(1 - e^{-\beta r})$,

$$\tag{A1}$$

D state: $w(r) = N\sin\epsilon\, e^{-\alpha r} v^2(r)\left[1 + \frac{3v(r)}{\alpha r} + \frac{3v^2(r)}{\alpha^2 r^2}\right]$,

$$\tag{A2}$$

where

$$v(r) = 1 - e^{-\mu' \alpha r} \quad \text{and} \quad \alpha^2 = \tfrac{1}{2} E_B (M_n + M_p).$$

E_B is the deuteron binding energy. $e^{-\alpha r}$ dominates the asymptotic behavior of u and w. A discussion of the determination of the remaining constants can be found elsewhere.[33] The momentum wave functions needed for the triple-differential cross section are:

$$\tilde{u}(k) = \int_0^\infty j_0(kr) u(r) r \, dr$$

$$= N \cos\epsilon \left[\frac{1}{k^2 + \alpha^2} - \frac{1}{k^2 + \beta^2} + \frac{1}{k^2 + 4\beta^2} - \frac{1}{k^2 + (\alpha+\beta)^2} \right], \tag{A3}$$

$$\tilde{w}(k) = \int_0^\infty j_2(kr) w(r) r \, dr$$

$$= N \sin\epsilon \left\{ \frac{1}{k^2} \left[I_1(a_0) - 2I_1(a_1) + I_1(a_2) \right] + \frac{3}{\alpha k} \left[I_0(a_0) - 3I_0(a_1) + 3I_0(a_2) - I_0(a_3) \right] \right.$$

$$\left. + \frac{3}{\alpha^2} \left[I_{-1}(a_0) - 4I_{-1}(a_1) + 6I_{-1}(a_2) - 4I_{-1}(a_3) + I_{-1}(a_4) \right] \right\}, \tag{A4}$$

where

$$a_m = (\alpha/k)(1 + m\mu') \quad \text{and} \quad I_n(a) = \int_0^\infty j_2(z) e^{-az} z^n dz.$$

Explicitly:

$$I_{-1}(a) = \tfrac{1}{2} a^2 + \tfrac{1}{3} - \tfrac{1}{2} a(a^2 + 1) \text{arccot} a, \tag{A5}$$

$$I_0(a) = -\tfrac{7}{4} a + \tfrac{1}{2}(3a^2 + 1) \text{arccot} a, \tag{A6}$$

$$I_1(a) = \frac{3a^2 + 2}{(a^2 + 1)} - 3 \, \text{arccot} a. \tag{A7}$$

In the above expressions arccot$a$ ranges from 0 to $\tfrac{1}{2}\pi$.

The integration over the c.m. angle ω^* has been done for the S state. Using for k the laboratory momentum of the spectator nucleon k_n:

$$\int_{\cos\omega^*_{\max}}^1 F^2(\omega^*) d(\cos\omega^*) = \int F^2(\omega^*) \frac{d(k_n^2)}{2\gamma^* \beta^* p^* E_n}$$

$$= \frac{N^2 \cos^2\epsilon}{2\gamma^* \beta^* p^*} \left[I(\gamma_1, \gamma_1) + I(\gamma_2, \gamma_2) + I(\gamma_3, \gamma_3) + I(\gamma_4, \gamma_4) - 2I(\gamma_1, \gamma_2) + 2I(\gamma_1, \gamma_3) \right.$$

$$\left. - 2I(\gamma_1, \gamma_4) - 2I(\gamma_2, \gamma_3) + 2I(\gamma_2, \gamma_4) - 2I(\gamma_3, \gamma_4) \right], \tag{A8}$$

where

$$\gamma_1 = \alpha, \quad \gamma_2 = \beta, \quad \gamma_3 = 2\beta, \quad \gamma_4 = \alpha + \beta,$$

and $\gamma^* = (1 - \beta^{*2})^{-1/2}$, $\beta^* c = $ velocity of the c.m. system with respect to the laboratory frame, E_n $= (M_n^2 + k_n^2)^{1/2} = $ total energy of neutron in the laboratory, $p^* = $ c.m. nucleon momentum. The I's are:

$$I(\gamma_1, \gamma_2) = \frac{1}{\eta_1^2} \left[T(\gamma_1) - \left(\frac{E}{E^2 - \eta_1^2} \right)_{E_{\max}}^{E_{\min}} \right], \quad \text{when } \gamma_1 = \gamma_2$$

or

$$= \frac{1}{\gamma_2^2 - \gamma_1^2} \left[T(\gamma_2) - T(\gamma_1) \right], \quad \text{when } \gamma_1 \neq \gamma_2$$

where

$$T(\gamma_1) = \left[\frac{1}{2\eta_1} \ln \frac{E + \eta_1}{E - \eta_1} \right]_{E_{\max}}^{E_{\min}}, \quad \eta_1 = (M_n^2 - \gamma_1^2)^{1/2}.$$

$E_{\max}$ is the neutron energy in the laboratory at $\omega^*_{\max}$ and $E_{\min}$ corresponds to $\omega^* = 0$. The integration over all ω^* is obtained by setting $E_{\max}$ equal to E_n, corresponding to $\omega^* = 180°$. This gives the S-state contribution to the double-differential cross section.

APPENDIX B

Additional data runs were taken at $\theta = 20°$ for q^2 = 5 amd 7 F^{-2}. These runs were taken to verify and extend the low-q^2 measurements made by Budnitz et al.[1] The basic apparatus used in these runs was the same as that used by Budnitz and by Goitein et al.[15] However, several improvements were made in the apparatus as described below. The results obtained from these measurements essentially agree with those obtained by Budnitz. It is found that the theory of Renard et al.[5] satis- factorily explains the proton coincidence results, whereas the McGee theory[4] without final-state interactions (FSI) does not.

The following improvements were made to the setup used by Budnitz:

(a) The electron momentum resolution was im- proved by limiting the electron acceptance to the steeper rays and by use of the upper trajectory through the quadrupole instead of the lower one. The FWHM resolution was thus decreased from 2.7% to 1.6% at $q^2 = 7$ F^{-2}.

(b) The proton spatial resolution was improved, particularly in the hodoscope, by eliminating the thin lead shielding placed in front of the proton detectors by Budnitz. Instead, a wide aperture magnet was used to reduce charged-particle back- grounds.

(c) The elimination of the lead absorber in front of the proton counters also reduced the size of the necessary corrections for proton absorption and neutron conversion.

(d) Improvements were made in the proton coin- cidence circuitry which allowed their operation at higher randoms probabilities, and hence allowed higher data-taking rates.

(e) At $q^2 = 7$ F^{-2} the recoil deuteron from the elastic e-d scattering process was detected in a small counter placed in front of the proton coun- ters.

(f) Background runs were taken with a lead sheet about three radiation lengths thick in front of the quadrupole magnet. These runs showed that there was negligible contamination from charged pions.

In order to make use of a magnet instead of the lead absorber used by Budnitz to reduce the rates in the proton counters, the size of the solid angle subtended by the proton counters was made slightly smaller than that subtended by the Budnitz setup. This reduction in solid angle slightly increases the size of the theoretical corrections; the change to the correction to f_p given by the McGee theory without FSI increases from 1.009 to 1.012 at $q^2 = 7$ F^{-2}. This is not a significant problem compared with the size of the corrections which appear to arise from FSI. Another small difference existed

because the edge of the proton detector was de- fined by lead instead of the edge of a scintillator. This has a negligible effect on f_p, however, since the fraction of quasielastic events with either a proton or neutron in the angular region near the edge of the detector is extremely small.

A study of the hodoscope data taken on D_2 indi- cated a substantial H_2 contamination in the target amounting to about 4.7%. Unfortunately this con- tamination was discovered after the D_2 used in the data runs was disposed of. Consequently the H_2 contamination could not be substantiated by direct analysis of the gas. The hodoscope data, however, provide very good evidence for the presence of this contamination and allow us to determine its magnitude to better than $\frac{1}{3}$ of its amount.

The analysis of the 20° data proceeded in a manner similar to that for the 90° data described in the body of this paper. Only slight modifications to the computer programs were necessary to change the specifications of the electron spectrom- eter.

The momentum spectra of the scattered electrons obtained on hydrogen are found to agree well with fits of the type described in Sec. IV D. The mea- sured spectra drop cleanly to zero above the elas- tic peak indicating the absence of background in that region.

The momentum spectrum measured on deuterium at $q^2 = 7$ F^{-2} is shown in Fig. 12. In obtaining the theoretical fits shown, only the normalization is al- lowed to vary. The momentum scale is determined by the elastic e-p peak measured on hydrogen. The theory of Renard et al. is seen to follow the data more closely than does the theory of McGee, as was observed also at $\theta = 90°$. It should be pointed
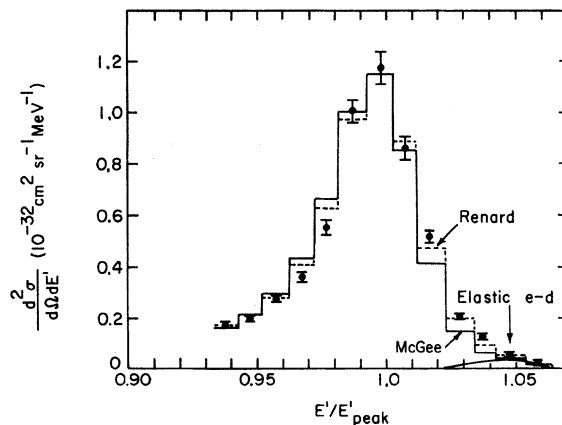

FIG. 12. Scattered electron momentum spectrum from deuterium at $q^2 = 7$ F^{-2}, $\theta = 20°$. The theoretical curves predicted by McGee (solid lines) and Renard et al. (dashed line) include the contribution from the elastic e-d process, which is also shown separately.

out, however, that the resolution function contributes substantially to the shape of the distribution here so that this does not provide a good test of the theory. Budnitz *et al.*[1] found that their measured momentum distribution at $q^2 = 7$ F^{-2} was narrower than predicted by the McGee theory after being folded with their considerably wider resolution function. This discrepancy does not appear in the present data. Good agreement with the momentum spectrum on D_2 at $q^2 = 5$ F^{-2} can only be obtained after the theoretical distributions are shifted by about 0.7% in E' relative to the elastic peak from H_2. It is thought that this shift in the momentum spectrum which was measured for the upper trajectory through the quadrupole, was produced by a slight (0.5 mm) displacement in the vertical position of the beam between the H_2 and D_2 runs. Unfortunately the spectrum for the lower trajectory, for which such a displacement in beam position would result in a shift in the opposite
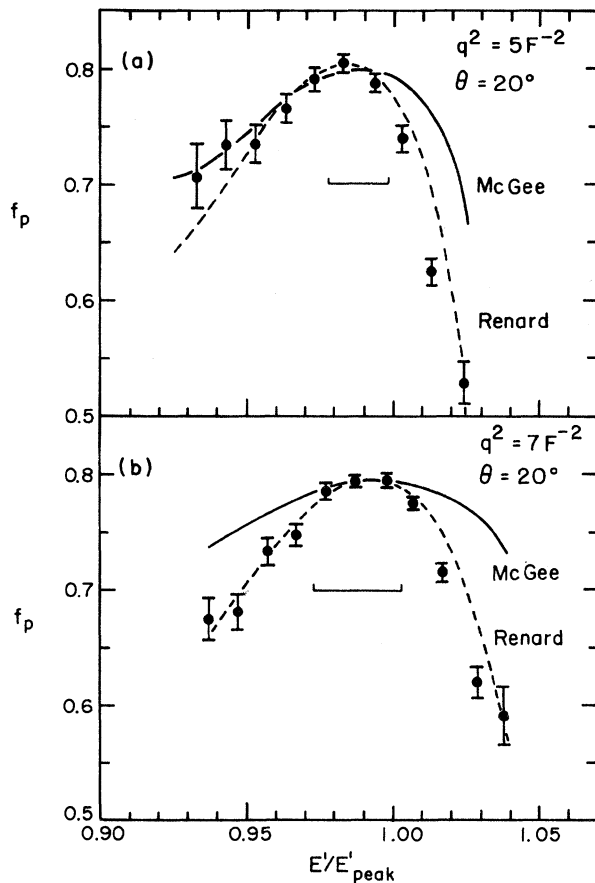
direction, is not available. At $q^2 = 7$ F^{-2}, where both trajectories are available, this possibility is excluded.

The contribution from the elastic e-d scattering process is shown separately in Fig. 12. Its contribution is calculated on the basis of previous measurements of the deuteron form factors.[16] At $q^2 = 7$ F^{-2} where the recoil deuteron was detected in coincidence with the scattered electron, the measured contribution to within about 20%.

Figure 13 shows the experimentally measured variation of the fraction of the electron events with a proton coincidence f_p with E'/E'_{peak} at $q^2 = 5$ and 7 F^{-2}. The comments in Sec. V F apply equally well to this figure. The effective cone angles subtended by the proton counters are given in Table IX (see Sec. V F). The observed variation of f_p with E' is in agreement with that observed by Budnitz *et al.*[1] The theoretical curves shown include the effects of the experimental setup and thus may be directly compared with the experimental results. The theoretical curves at $q^2 = 5$ F^{-2} have been offset by 0.7% in E' to correspond to the offset observed in the momentum spectrum. It is seen that the Renard theory predicts a variation of f_p with E' which follows the data much more closely than that predicted by the McGee theory, especially at values of E' which lie above the quasielastic peak. This agreement is also observed at $\theta = 90°$ and is thought to be partially due to the inclusion of FSI in the Renard theory. The McGee theory used here does not include FSI effects (Sec. II A). It appears that the Renard theory adequately explains these proton coinci-

FIG. 13. f_p, the fraction of events with a proton coincidence, vs E' (a) at $q^2 = 5$ F^{-2} and (b) $q^2 = 7$ F^{-2}; both for $\theta = 20°$. The theoretical predictions of McGee and of Renard *et al.* are shown. The brackets indicate the momentum bite used in proton coincidence method.

TABLE IX. Effective ω_{lab} subtended by proton counters for $\theta = 90°$.

$E'/E'_{\text{H}_2 \text{ peak}}$	Effective ω_{lab} (deg)	
	$q^2 = 5$ F^{-2}	7 F^{-2}
1.04	$\cdots$	17.9
1.03	17.0	20.3
1.02	20.8	20.6
1.01	21.1	21.0
1.00	21.2	21.1
0.99	21.2	21.2
0.98	21.0	20.9
0.97	20.8	20.7
0.96	20.3	20.3
0.95	19.8	19.7
0.94	19.2	19.1
0.93	18.5	18.3

dence results.

The proton coincidence data on D_2 have been used to determine σ_p as described in Sec. V E. The values of $(\sigma_p)_{D_2}/\sigma_p$ obtained by the area method are given in Table X. A discussion of the entries in this table is given in Sec. V E. The McGee theory without FSI is used to make the theoretical corrections. No subtractions are necessary for the reverse-field and empty-target backgrounds. The excess $e\bar{p}$ events observed in the H_2 runs at 90° are found to be essentially nonexistent at 20°; at $q^2 = 7$ F^{-2} the excess $e\bar{p}$'s are determined to be $(0.01 \pm 0.16)\%$, or are consistent with zero. The error in the elastic e-d subtraction is assigned to be $\frac{1}{3}$ of its magnitude. The uncertainties in the Cherenkov and shower counter efficiencies are negligible and are not listed in Table X. The final result at $q^2 = 7$ F^{-2} is in agreement with that obtained by Budnitz et al.[1]: 0.910 ± 0.008 (after multiplying their value by 0.990 to correct for the new deuteron wave functions used here). The result at $q^2 = 5$ F^{-2} is essentially the same. The interpretation of these results in terms of the appropriate theory to analyze the proton coincidence data was discussed in Sec. V E.

The peak method has also been used to analyze the proton coincidence data to obtain $(\sigma_p)_{D_2}/\sigma_p$. Using the McGee theory with no corrections for FSI effects yields 0.953 ± 0.050 at $q^2 = 7$ F^{-2}. The

TABLE X. $(\sigma_p)_{D_2}$: Area method applied to D_2 coincidence data.

q^2 (F^{-2})	5.0	7.0
θ (deg)	20	20
Momentum bite:		
E'_{min}/E'_{peak}	0.931	0.933
E'_{max}/E'_{peak}	1.062	1.064
$(\sigma_p)_{D_2}/\sigma_p$	0.916	0.921
Theoretical corr.		
Integrated $(d^2\sigma/d\Omega\,dE')_{coin}/\sigma_p$	0.900	0.921
Rad. corr. factor	1.163	1.167
Exp. corr. to area		
H_2 contamination subtraction	0%	0%
Elastic e-d subtraction	0.0%	−1.1%
Corrections to σ_p		
Momentum bite:		
E'_{min}/E'_{peak}	0.941	0.931
E'_{max}/E'_{peak}	1.039	1.062
Rad. corr. factor (including resolution)	1.162	1.147
Errors in $(\sigma_p)_{D_2}/\sigma_p$		
Statistics	1.6%	0.9%
Momentum bite	2.2%	1.0%
Beam monitoring	1.0%	1.0%
Background subtractions	0.3%	0.4%
Net error	2.3%	1.7%

TABLE XI. $(\sigma_n + \sigma_p)/\sigma_p$: Area method.

q^2 (F^{-2})	5.0	7.0
θ (deg)	20	20
Momentum bite:		
E'_{min}/E'_{peak}	0.931	0.933
E'_{max}/E'_{peak}	1.062	1.064
$(\sigma_n + \sigma_p)/\sigma_p$ (after all corr.)	1.163	1.189
Theoretical corr.		
Integrated $(d^2\sigma/d\Omega\,dE')/(\sigma_n + \sigma_p)$	0.955	0.968
Rad. corr. factor	1.163	1.169
Exp. corr. to area		
H_2 contamination subtraction	+ 0.8%	+ 0.9%
Elastic e-d subtraction	−2.6%	−1.1%
Errors in $(\sigma_n + \sigma_p)/\sigma_p$		
Statistics	1.6%	0.7%
Momentum bite	1.2%	0.7%
Beam monitoring	1.0%	1.0%
Background subtractions	0.6%	0.4%
Net error	2.3%	1.5%

correction for the momentum resolution amounts to 12% with an estimated error of about 4%. This result is consistent with those obtained at 90°.

The values of $(\sigma_n + \sigma_p)/\sigma_p$ obtained by the area method and by the proton coincidence method are presented in Tables XI and XII. The analysis of the data proceeds along the same lines as discussed in Secs. V D and V G, respectively. The McGee theory is used in the area method with no correction for FSI. The result at $q^2 = 7$ F^{-2} is in

TABLE XII. $(\sigma_n + \sigma_p)/\sigma_p$: Proton coincidence method.

q^2 (F^{-2})		5.0	7.0
θ (deg)		20	20
Momentum bite:			
E'_{min}/E'_{peak}		0.985	0.973
E'_{max}/E'_{peak}		1.005	1.003
$(\sigma_n + \sigma_p)/\sigma_p$ (after all corr.):	McGee	1.218	1.240
	Renard	1.174	1.197
Theoretical corr.			
Corr. factor to f_p:	McGee	1.031	1.018
	Renard	1.070	1.053
Exp. corrections			
Randoms prob.		4.3%	5.1%
Proton counter efficiency		1.88%	2.04%
Neutron conversion prob.		0.3%	0.3%
Effect on $(\sigma_n + \sigma_p)/\sigma_p$ of subtractions:			
H_2 contamination subtraction		1.5%	1.2%
Errors in $(\sigma_n + \sigma_p)/\sigma_p$			
Statistics		0.7%	0.4%
Background subtractions		0.5%	0.4%
Proton counter efficiency		0.3%	0.2%
Randoms corr.		0.4%	0.5%
Net error		1.0%	0.8%

agreement with that found by Budnitz *et al*.: 1.172 ±0.010 (after multiplication by 0.990 to take into the difference in deutron wave functions). As discussed in Sec. V F, the theory of Renard *et al*. is preferable for analyzing the proton coincidence data. The result obtained here at $q^2 = 7$ F^{-2} is consistent with that found by Budnitz when his result is corrected for use of the Renard theory: 1.211 ± 0.006. It is also found that the area method and proton coincidence method results are in mutual agreement at both $q^2 = 5$ and 7 F^{-2}.

At $q^2 = 5$ F^{-2} the area method result agrees with the value of $\sigma_n/\sigma_p = 0.152$ given by the "scaling law," and $G_{En} = \tau G_{Mn}/(1 + 4\tau)$, which should be a good representation of the form factors for small q^2. The value obtained by the proton coincidence method is almost two standard deviations higher

than this, however. This may be an indication of a breakdown in the proton coincidence method at low q^2, even when the theory of Renard *et al*. is used to interpret the proton coincidence data.

The values of $(\sigma_n + \sigma_p)/\sigma_p$ at $q^2 = 4.6$ F^{-2} of Hughes *et al*.[13] have been decreased by 4.3% to correspond to the theoretical interpretation used in the present work, and have been increased by about 0.005 to change to $q^2 = 5$ F^{-2} for comparison with the present results. It is found that the data of Hughes *et al*. are inconsistent with the present results and diverge from a reasonable form-factor fit as θ approaches zero in much the same way as is shown in Fig. 9(a) for $q^2 = 10$ F^{-2}. Unfortunately, no other data exist for large values of θ, so it is not possible to perform a fit to extract the neutron form factors.

---

*Work supported by the U.S. Atomic Energy Commission.

†Presently at Cornell University, Ithaca, New York.

‡Presently at California State College at Sonoma, Rohnert Park, California.

§Presently at Department of Radiotherapy, Massachusetts General Hospital, Boston, Mass.

∥Presently at University of Illinois, Urbana, Ill.

**Presently at Columbia University, New York, New York.

[1] R. J. Budnitz, J. Appel, L. Carroll, J. Chen, J. R. Dunning, Jr., M. Goitein, K. Hanson, D. Imrie, C. Mistretta, J. K. Walker, and R. Wilson, Phys. Rev. **173**, 1357 (1968).

[2] L. E. Price, J. R. Dunning, Jr., M. Goitein, K. Hanson, T. Kirk, and Richard Wilson, Phys. Rev. D **4**, 45 (1971).

[3] K. Hanson, Ph.D. thesis, Harvard University, 1970 (unpublished).

[4] I. McGee, Phys. Rev. **158**, 1500 (1967).

[5] F. M. Renard, J. Tran Thanh Van, and M. Le Bellac, Nuovo Cimento **38**, 552 (1965); Nuovo Cimento **38**, 565 (1965); Nuovo Cimento **38**, 1688 (1965).

[6] L. Durand, Phys. Rev. **115**, 1020 (1959).

[7] L. Durand, Phys. Rev. **123**, 1393 (1961).

[8] R. Blankenbecler and L. F. Cook, Phys. Rev. **119**, 1745 (1960).

[9] T. Houk and R. Wilson, Rev. Mod. Phys. **39**, 546 (1967); see also Rev. Mod. Phys. **40**, 672(E) (1968).

[10] M. N. Rosenbluth, Phys. Rev. **79**, 615 (1950).

[11] D. Braess and G. Kramer, Z. Phys. **189**, 242 (1966).

[12] I. McGee, Phys. Rev. **161**, 1640 (1967).

[13] E. B. Hughes, T. A. Griffy, M. R. Yearian, and R. Hofstadter, Phys. Rev. **139**, B458 (1965).

[14] J. Nutall and M. L. Whippman, Phys. Rev. **130**, 2495 (1963).

[15] M. Goitein, R. J. Budnitz, L. Carroll, J. R. Chen, J. R. Dunning, Jr., K. Hanson, D. C. Imrie, C. Mistretta, and Richard Wilson, Phys. Rev. D **1**, 2449 (1970).

[16] C. D. Buchanan and M. R. Yearian, Phys. Rev. Lett. **15**, 303 (1965).

[17] G. C. Hartman, Ph.D. thesis, Massachusetts Institute of Technology, 1967 (unpublished).

[18] S. Adler, Ann. Phys. (N.Y.) **50**, 189 (1968).

[19] N. Meister and T. Griffy, Phys. Rev. **133**, B1032 (1964).

[20] L. W. Mo and Y. S. Tsai, Rev. Mod. Phys. **41**, 205 (1969).

[21] N. Meister and D. R. Yennie, Phys. Rev. **130**, 1210 (1963).

[22] W. T. Scott, Rev. Mod. Phys. **35**, 231 (1965).

[23] R. J. Tapper, Rutherford High Energy Laboratory Internal Report No. NIRL/R/95, 1965 (unpublished).

[24] W. Bartel, F. W. Büssen, W.-R. Dix, R. Felst, D. Harms, H. Krehbiel, P. E. Kuhlmann, J. McElroy, W. Schmidt, V. Walther, and G. Weber, Phys. Lett. **30B**, 285 (1969).

[25] W. Bartel *et al*. reported by R. Wilson, in *Proceedings of the 1971 International Symposium on Electron and Photon Interactions at High Energies*, edited by N. B. Mistry (Laboratory of Nuclear Studies, Cornell University, Ithaca, N.Y., 1972) and DESY Report No. DESY 73/5 (unpublished).

[26] P. Stein, M. Binkley, R. McAllister, A. suri, and W. Woodward, Phys. Rev. Lett. **16**, 592 (1966).

[27] W. Albrecht, H.-J. Behrend, H. Dorner, W. Flauger, and H. Hultshig, Phys. Lett. 26B, 642 (1968).

[28] S. Galster, G. Hartwig, H. Klein, J. Moritz, K. H. Schmidt, W. Schmidt-Parzefall, D. Wegener, and J. Bleckwenn, Kernsforschungszentrums Karlsruhe Report No. KFK 1473, 1971 (unpublished).

[29] C. W. Akerlof, K. Berkelman, G. Rouse, and M. Tigner, Phys. Rev. **135**, B810 (1964).

[30] V. Krohn and G. Ringo, Phys. Rev. **148**, 1303 (1966).

[31] B. Casper and F. Gross, Phys. Rev. **155**, 1607 (1967).

[32] S. Galster, H. Klein, J. Moritz, K. H. Schmidt, D. Wegener, and J. Bleckwenn, Nucl Phys. B32, 221 (1971).

[33] Reference 1, and Richard Wilson, *The Nucleon-Nucleon Interaction* (Wiley, New York, 1963), Chap. 2. It should be noted that some of the approximations made in the latter, notably Eq. (2-59), are inadequate for accurate calculations.